Published in "Physica Scripta 88(6): 068511, 2014"
which should be cited to refer to this work.

Future directions of μSR—laser excitation

K Yokoyama[1,2], P Murahari[1,2], P Heathcote[3], L Nuccio[4], J S Lord[2], N A Morley[5] and A J Drew[1,2]

[1] School of Physics and Astronomy, Queen Mary University of London, Mile End Road, London E1 4NS, UK
[2] ISIS Pulsed Muon Facility, STFC Rutherford Appleton Laboratory, Harwell Oxford, Didcot, Oxfordshire OX11 0QX, UK
[3] School of Biological and Chemical Sciences, Queen Mary University of London, Mile End Road, London E1 4NS, UK
[4] Department of Physics and FriMAT, University of Fribourg, Chemin du Musée, Fribourg CH-1700, Switzerland
[5] Department of Materials Science and Engineering, University of Sheffield, Mappin Street, Sheffield S1 3JD, UK

E-mail: a.j.drew@qmul.ac.uk

Abstract

We discuss the general principles of laser-excited muon pump–probe spin spectroscopy (photo-μSR), including the historical origins of the technique, and discuss the overall experimental method. We review examples of past work using this technique, then discuss the future upgrade of the HiFi spectrometer with a high-power laser system. In particular, we note that performing photo-μSR experiments at high field around avoided level crossing resonances in unsaturated organic materials, offers advantages over the work previously performed at lower magnetic fields. We then present some results from some preliminary modelling of a rather simple two-electron spin system, where we see quite a complicated behaviour of the avoided level crossings. Finally, we discuss some potential applications in the biosciences, such as electron transfer in peptides and photochemistry of carotenoids, as well as magnetism which is a more traditional area for study with muons.

1. Introduction

Muon spin spectroscopy (collectively known as μSR, corresponding to muon spin relaxation, resonance or rotation) has shown itself to be a very powerful probe of material properties, with major activities directed towards understanding superconductors, various classes of magnetic materials, semiconductors and organic materials. It is worth noting that it is possible to perform experiments with both negatively charged muons and positively charged anti-muons. However, the positively charged anti-muon, which within the μSR community is generally referred to as a muon (dropping the 'anti'), is the most extensively used variety of muons due to the possibility of using them as a probe of material properties. Indeed, from this point forward, we will continue with the (incorrect) convention of using the term 'muon' for the positively charged variety. Detailed information about some of the work in these areas, and the general background to the muon technique, can be found elsewhere in this issue and in other reviews (see e.g. [1–7]). However, at this point it is worth noting that muons can behave quite differently depending on the material they are implanted in. For example, in metals a bare positively charged muon is the stable state. In the case of semiconductors, dielectrics and molecular compounds, a large fraction of muons are often found in a stable bound state with an electron, i.e. the so-called muonium atom is observed. In an organic sample, muonium can form a bond with the molecules in the last step of the thermalization process, joining a molecule at a site with high electron concentration, such as unsaturated bonds or aromatic rings. These are often referred to as muoniated radicals. Throughout this paper, we use the following terminology—μ^+ to mean

a bare, positively charged muon; Mu to mean a muonium atom, in whatever state it finds itself in the material; and Mu^- to mean a negatively charged muonium—a muon with two electrons.

In the context of the future photo-excited μSR (photo-μSR) on the organic materials that are discussed here, it is the muoniated radical that is the primary probe of photo-excited dynamics. Importantly, despite the availability of a laser on a muon spectrometer, remarkably little work has been done to study the dynamics of excited states. Some pertinent examples exist, normally involving muonium in one of its guises, but the systems studied are not as widespread as one may have expected. This may be partially related to the maximum magnetic field available on the current spectrometers, which limits the level of information available in systems with muoniated radicals. It is also clear that laser-pump muon-probe experiments are extremely technically challenging, for example there is a major problem ensuring the light absorption profile matches the muons stopping profile. Studying muoniated radicals in solution at high magnetic fields may alleviate some of these experimental problems and aid the interpretation of the data, but the liquid experiments themselves bring additional experimental challenges. Nonetheless, perhaps the upgrade with a laser on the high magnetic field spectrometer at the ISIS Pulsed Muon Source will broaden the appeal and impact of the photo-μSR technique.

1.1. General principle

Historically, pulsed muon sources have been preferably utilized to conduct photo-μSR experiments because, firstly, a full time spectrum of muon decay can be observed so that one can trace the even slow muon dynamics induced by the laser illumination, and secondly, it can be easily coupled to the laser system for pulsed stimulation by synching the pulse timings. With the pulsed muon source, the laser-induced change of material can be a slow process which, in principle, can be extended out to the muon pulse separation time (in the order of 20 ms). This feature is considered to be particularly important in the field of chemistry and biochemistry, where some of the chemical reactions are relatively slow. By changing the trigger timings, the laser pulse can illuminate on the sample before or after the muon pulse, which enables one to observe the dynamics at an arbitrary timing.

For such a system, the laser source needs to be short-pulsed, high-power, wavelength-tuneable and probably narrow-linewidth for high-resolution spectroscopy. Considering these conditions, it is the best suited to utilize an optical parametric oscillator (OPO) pumped by a Nd:YAG Q-switched pulsed laser system. The laser system is tuneable in wavelength by changing the phase-matching angle of the OPO crystals, and produces a pulse duration typically in the order of ns and a pulse energy ranging from several mJ to 100 mJ per pulse depending on the output wavelength [9]. The linewidth of the OPO output is typically in the order of a few hundreds of GHz, which is sufficient for most of the applications in condensed matter, where the energy spectra are already homogeneously/inhomogeneously broadened. However the YAG fundamental (1064 nm) and harmonics (532, 355, 266, 213 nm) could be narrowed down to the order of 0.1 GHz when the YAG oscillator is injection-seeded. Another advantage of using such system is that the repetition rate of the laser system is similar to the accelerator. The pulsed laser systems used so far in RAL and KEK run on a half of the accelerator repetition rate so that there are two modes in the data; laser ON and OFF mode. Because the general approach of the method is to observe the difference in these two modes, it protects against some of the systematic errors. As discussed later, it is also possible to make circularly polarized light and change its helicity alternately, where one also observes the difference in the signal depending on the laser light to be circularly polarized either in left- or right-handed. This is also something only a pulsed system can do.

It is important to note that extra care needs to be taken for the sample holder for photo-μSR experiments. Firstly the sample holder generally has two windows; the muon and laser windows. As is the same for other sample holders for μSR experiments, the muon window needs to be thin enough so that the incident muon beam can penetrate through the window to be implanted in the sample. On the other hand, the laser window needs to be transparent at the given laser wavelength. If the muon and laser beam are incident on the same side of the sample holder (by tilting the sample holder, for example), then the window can be a thin sheet of quartz (such as 200 μm thick) to satisfy both conditions. Secondly it is important to make sure that the density distribution of the absorbed photons in the material has enough spatial overlap with the muon distribution. The muons are implanted in material and spatially distributed in a roughly Gaussian profile, whereas the photons are absorbed exponentially with the absorption coefficient α. Therefore one needs to know the absorption spectrum of the sample and tune the laser wavelength so that α is the correct value, such that the photon absorption has a good spatial overlap with respect to the muon distribution. Obviously it becomes more difficult to satisfy the condition as the interested wavelength becomes shorter because materials becomes more absorbent in the UV range. Moreover, if there are multiple optical bands at similar wavelengths, satisfying this condition may be rather challenging. For example, it could be that to match the light absorption with the muon stopping profile, the laser would have to be tuned so far away from the relevant absorption band that the yield of the excitation of interest is too small. Thirdly, laser heating can be another problem especially when the experiment requires a high laser power. Since the absorption of the pump laser acts to heat the sample, the sample temperature will keep increasing unless there is a heat sink. When the laser power is large, one needs to start thinking about how to dump the laser beam safely. Because the sample space is generally quite tight and small in the muon spectrometers, the solution may be to dump the beam outside the spectrometer by reflecting and routing the laser beam.

1.2. The history of photo-excited μSR experiments

Before the laser came into play, researchers used flash lamps to perform photo-μSR experiments. Even today the flash lamp is a handy and easy method to photo-excite samples because

the laser system tends to be costly, takes up more space and requires higher safety protocol. However, drawbacks are of course the low power, long pulse duration (tens of μs) and broad spectrum. One of the first photo-excited μSR experiments was performed by Kadono *et al* [10] to study the muonium (Mu) states in Si and Ge undergoing Mu charge-exchange reaction under photoexcitation. They studied how the Mu species (such as the tetrahedral interstitial Mu state and the bond-centred Mu state) are interchanged and converted to the different ones when mediated by the photoinduced electrons. More recently Jayasooriya *et al* [11] applied the flash lamp excitation on crystalline benzophenone to study the hyperfine (HF) coupling tensor of Mu radical using the avoided level crossing (ALC) technique. They measured a small change in the signal probably because the spectral density of light was too low.

The first laser experiment was performed by Shimomura *et al* [12] in 1999 at KEK in Japan, where they installed a flash lamp pumped Ti:sapphire laser, generating a few tens of ns laser pulses at 750–860 nm. There they studied the minority carrier processes in GaAs by observing a reduction in the muon asymmetry upon the laser illumination. They found an anomalous transport phenomenon where the photo excited effect is extended deep into the sample compared with the expected photo-absorption depth. They considered the reason was due to the photon recycling process, one of the candidates of the minority carrier process. Using the same facility Torikai *et al* [13] pioneered the study of electron spin exchange scattering in GaAs, which gave the basic principle in the experiment detailed in the following sections.

1.3. Existing facilities: RIKEN-RAL Port-2

The RIKEN-RAL Port-2 in ISIS facility in the UK is currently the only muon beam line with a laser setup, where one can perform the photo-μSR experiments. The laser system is based on the OPO (Continuum Panther EX OPO) pumped by a high-power Nd:YAG laser system (Continuum Powerlite 9025). The OPO takes 355 nm for pump laser and the OPO signal and idler can be frequency doubled to generate the second harmonic wavelength in the UV range. Therefore the output wavelengths cover almost the whole spectrum ranging from 210 to 2200 nm except the degeneracy wavelength at 710 nm. Although the pulse energy depends on the output wavelength, the peak pulse energies are 50 mJ per pulse at 405 nm for the signal, and 20 mJ per pulse at 840 nm for the idler. If the YAG oscillator is not seeded, the pulse duration is typically 6 ns, and the linewidth is approximately 150 GHz at 405 nm. The laser system runs at 25 Hz, and a Q-switch in the YAG oscillator is triggered by the signal from the accelerator to synchronize the muon and laser pulse. The near-field beam profile is top-hat with an elliptical shape. However, since the laser beam propagates along a light-tight beam duct connecting the laser cabin and the spectrometer, the beam profile is deformed by the time it reaches the sample because of the multi-transverse mode structure of the laser profile. For some experiments, such as the one performed by Bakule *et al* [14], it is important to maintain the good beam profile for the more uniform spacial distribution of photons. In such case an image relay setup gives a solution, where a pair of long-focal distance positive lenses images the beam profile in one end of the telescope to another.

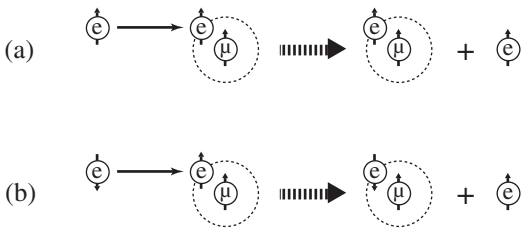

Figure 1. Spin exchange scattering between the photo-induced conduction electron and Mu in triplet state with $m_F = +1$. (a) When the conduction electron spin is parallel to the muon spin, the spin exchange interaction does not affect the spin state. (b) When the electron spin orientation is anti-parallel, the Mu spin results in $m_F = 0$ so that the muon spin polarization is quickly lost because of the electron–muon HF interaction.

2. The first successful measurements

This section reviews some of the first photo-μSR measurements performed at the RIKEN-RAL Port-2. More focus is put on the spintronics experiment on GaAs because it illustrates the basic principles of the photo-μSR experiment, and its methodology is considered to be relatively general for many μSR applications. It is also suitable to illustrate the method utilizing not only the laser illumination but also the light helicity to optically induce the electron spin.

2.1. Spintronics experiment on GaAs

2.1.1. Overview and principle of the experiment. In the field of semiconductor spintronics, many researchers are looking for materials with long electron spin lifetime and easy spin manipulation. Among many semiconducting materials, C, Si and Ge are considered to have a prolonged spin lifetime because they are light atoms and do not have a nuclear magnetic moment (although there are some exceptions in their isotopes). They are obviously important semiconductors in terms of their natural abundance and easiness of fabrication. However it is difficult to characterize the conduction electron spin behaviour in these semiconductors because they have indirect band gap and weak spin–orbit coupling, which make the common optical techniques difficult to apply. On the other hand Mu can be sensitive to the conduction electron spin orientation by the spin exchange scattering between its bound electron and conduction electron. It is also well-known that Mu is present in most of the semiconducting materials. As shown in figure 1, when a Mu in triplet state with $m_F = +1$ collides with an electron with its spin parallel to the muon spin, the Pauli's exclusion principle prevents it from making any interactions, resulting in no change in the Mu state. However when the electron spin is antiparallel to the muon spin, then the conduction electron can be exchanged with the bound electron in Mu, changing the Mu state to $m_F = 0$. Since it is in a superposition of singlet and triplet $m_F = 0$, the muon spin oscillates between up and down state by the HF interaction. The muon spin is thus quickly depolarized, which results in reducing the muon asymmetry signal. Therefore in principle the μSR technique should be sensitive to the electron

spin orientation if there is enough interaction between Mu and conduction electrons.

To check feasibility of the principle, the researchers chose GaAs as a prototype sample because Si doped n-type GaAs has a relatively long electron spin lifetime (≈100 ns under low temperature) if the dopant concentration is at the right level (≈10^{16} cm^{-3}) [15]. The conduction electron spin polarization can be induced by optical spin orientation where the angular momentum of circularly polarized light is transferred to the spin angular momentum via the spin–orbit coupling, when the laser light (815 nm at 14 K) photo-excites electrons from the valence to conduction band. Properties of the electronic spin have been well-characterized in GaAs because of its large spin–orbit coupling, which makes it an ideal system for the feasibility studies. As described earlier, Torikai *et al* [13] pioneered the muon method in KEK, although the signal was too small to distinguish the change in the electron spin polarization. Yokoyama *et al* [16] revisited and addressed the problem by using more advanced optical techniques and the newly developed RIKEN Port-2 laser system.

2.1.2. Experimental setup and sample holder. In the experiment the muon and laser beam counter-propagate with each other towards the sample i.e. the muons are implanted from the 'front' side of the sample while the laser beam illuminates the sample from its 'back'. The sample, a n-GaAs wafer, is stored in a sample holder attached on a He-flow cryostat. The sample holder has a 125 μm thick aluminium window for the muon beam on one side, and a fused silica window for the laser beam on the other. The sample cell is made air-tight by the indium sealing so that it can be purged with He as a thermal exchange gas to uniformly cool down the sample wafer (350 μm thick, 2″ diameter). Because this mounting method does not clamp down the sample and just rest it under gravity, one can control the sample temperature without mechanical stress induced by contraction during the cooling process. It is known that the electron spin lifetime is affected by the mechanical stress, which makes it difficult to reproduce the same sample condition with the normal mounting methods, such as fixing with heat-conducting adhesive [17]. As stated above, to ensure the spatial overlap between the muon and laser light across the entire thickness of the wafer, the laser wavelength has been selected to 830 nm, where the photon energy is slightly below the band gap energy at 15 K (set as the typical temperature of the experiment). The wavelength has been selected not only by measuring the absorption spectrum of the sample but also by tuning the wavelength to maximize the OFF–ON signal as illustrated in the following section. The photons still can excite the electrons from the valence band to the conduction band with the photon energy because there are impurity states extended out from the valance and conduction band towards the centre of the band gap [18]. The photons with sub-gap energy photo-excite electrons both (i) from the impurity states above the valance band to the conduction band, and (ii) from the valance band to the impurity states below the conduction band. In the case (ii), the electrons in the donor impurity state are considered to be delocalized when the dopant concentration of n-GaAs is above the metal–insulator transition [19]. Therefore part of the electron spin excited

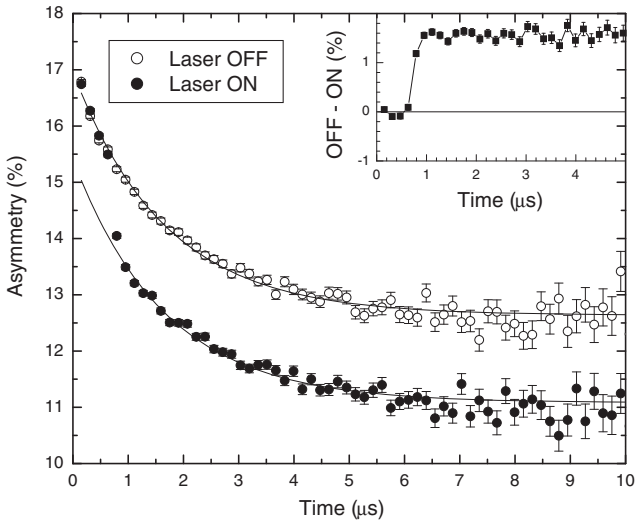

Figure 2. A typical longitudinal field (LF)-μSR time spectrum with and without the laser pulses ('ON' and 'OFF' mode) under 1000 G longitudinal magnetic field at $T = 15$ K. The laser energy is 1.3 mJ per pulse of 831 nm. Here in the laser ON mode, the light polarization can be considered as unpolarized because the data is an average of two modes: the laser light in left- and right-handed circular polarization.

in the donor impurity state should be exchanged with the conduction electrons.

The repetition rate of the laser is at 25 Hz, which thus makes the laser pulse incident on the sample every other muon pulse. Typical laser energy is approximately 1 mJ per pulse at 830 nm (illuminating approximately 8 cm^2), which is enough to photo-excite the electrons in the sample in the same level as the dopant concentration. The timing is set so that the laser pulse is on the sample about 0.9 μs after the muon pulse implantation as shown in figure 2. The laser pulse is circularly polarized by a quarter wave plate and its helicity is changed every other laser pulse by utilizing a Pockel's cell as a fast switch to flip the light helicity. The helicity change results in the change of the electron spin polarization, which is parallel to the muon spin in one helicity and anti-parallel in the other.

2.1.3. Data interpretation. Figure 2 shows the typical μSR time spectrum with and without the laser pulse ('ON' and 'OFF') under 1000 G longitudinal magnetic field at $T =$ 15 K. The OFF data is a normal μSR spectrum showing a relaxation of the tetrahedral interstitial site Mu relaxing due to the nuclear magnetic field associated with the surrounding atoms [20, 21]. When the laser pulse is illuminated at $t =$ 0.9 μs, the muon asymmetry suddenly decreases because the absorbed photons create photo excited electrons, which then interact with the Mu via spin exchange scattering. Because of the depolarizing mechanism described above, the conversion from the Mu triplet with $m_F = +1$ to 0 state results in the fast loss of muon spin asymmetry. This depolarization process can be clearly seen as an instantaneous drop of the muon spin asymmetry. An inset in figure 2 shows the difference, OFF–ON, to clearly see the reduction is step-like, without any relaxation, which suggests that Mu^- is responding to the photo-induced electrons [22].

When the laser light is circularly polarized, the amount of the step-like reduction depends on the helicity of the laser

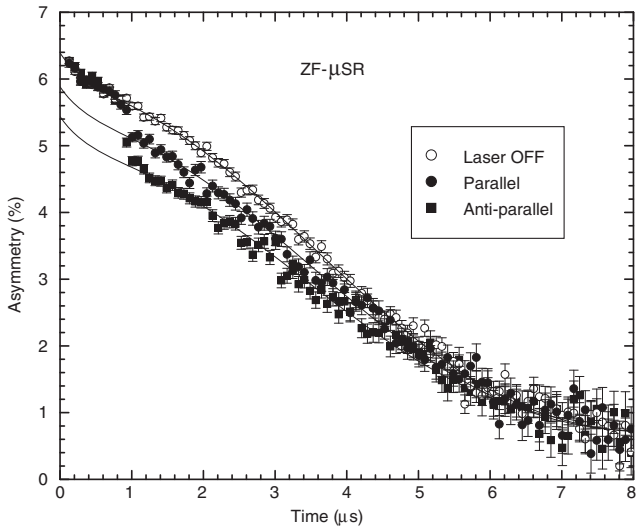

Figure 3. Zero field (ZF)-μSR time spectra for laser-OFF, parallel and antiparallel spin configuration under 0 G with laser energy 1.5 mJ per pulse and sample temperature at 15 K.

light. Figure 3 shows one of the first successful observations of Mu responding to different orientation of the optically induced electron spin [16, 22]. The signal is relatively small, but it can be clearly seen that the reduction of asymmetry is larger for the anti-parallel orientation and smaller for the parallel orientation, which is exactly what the model in figure 1 predicted. The signal has been confirmed that it follows the experimental parameters consistently along the predictions (such as the laser wavelength, intensity and sample temperature). After a series of experiments, Yokoyama *et al* [22] reported that the laser helicity effect is the largest when the longitudinal B-field is set to zero, and it is probably Mu^- responding to the optically induced spin. The maximum effect at $B = 0$ is consistent with the Mu depolarization mechanism described in figure 1 because the resulting Mu state is in a complete superposition of $m_F = 0$. However the fact that Mu^- is the species responding to the electron spin polarization is a puzzling problem, which requires further investigation. However it is an important step forward that the experiment proved that the μSR technique is capable of observing the electron spin polarization. It is expected that the technique can be applied to other semiconductors, and the application on Si is already underway.

2.2. Photo-ionization of muonium

There is another intriguing photo-μSR experiment performed on GaAs using the laser system in the RIKEN Port-2 beam line, with an aim to observe the direct interaction between Mu and photon. In terms of the energy level of Mu, it forms an impurity state in the band gap of GaAs. The energy level of the impurity state depends on the form of Mu, and Lichti *et al* [23] reported that Mu^- in GaAs forms an impurity state at 0.98 eV below the conduction band. When a photon with this amount of energy is illuminated on Mu^-, it is possible to remove its bound electron and excite it to the conduction band. If the laser light is unpolarized, the resulting Mu is either in $m_F = 0$ or +1. Therefore Mu with $m_F = 0$ is depolarized for the same reason as discussed above. Shimomura *et al* [24] have tuned the OPO laser system to the IR region and has observed the muon asymmetry drop as a function of the laser wavelength, with the largest asymmetry reduction at around 0.98 eV. They have concluded that this is the signal of the photo detachment of Mu^-, which is a common muon species in n-type semiconductors [25]. This experiment can be a general method to characterize the Mu impurity states in various semiconducting materials.

2.3. Reaction of Mu with excited H_2

The third example of the laser stimulated μSR experiment is on the reaction of Mu with vibrationally excited gaseous H_2 molecule [14]. The experiment is to measure the reaction rate λ for Mu + $H_2\{1\} \rightarrow$ MuH + H, where {1} denotes the vibrational quantum number $n = 1$. When muon is implanted in hydrogen gas, the muon captures an electron to form a Mu, which is a stable atom in the gas and the probability to react with another hydrogen molecule is low. However when the hydrogen molecule is in the excited state, the reaction rate is enhanced. This simple system is considered to be one of the most fundamental molecular systems to test the quantum mechanical calculations. To populate the excited state of hydrogen, the gas cell was pumped with an extremely intense 532 nm laser light to induce the stimulated Raman scattering [14]. The gas cell needs to be pressurized to stop the muon in a small volume so that the laser beam can be focused to achieve high intensity. Generally speaking, experiments with gas require higher laser power because of the less absorption compared with the case of condensed matters. Good agreement between the experiment and theory was shown, demonstrating that the technique can be a new tool to investigate the quantum mechanical behaviour for other chemical reactions in a gas.

2.4. Excited state chemistry

The only report of a photo-μSR experiment in the liquid state we are aware of was carried out by Ghandi *et al*. They studied short-lived excited states and transients created by pulsed laser excitation in water and rose bengal solution [26]. In the first experiment, a change in the diamagnetic muon fraction was observed in water upon irradiation with light at 532 nm, which is interpreted as confirming the role of hydrated electrons in the process of muonium formation in water. This supports the radiolysis model of muonium formation and is inconsistent with a pure hot atom model. The aim of the second study was to investigate the chemical dynamics of the reaction between Mu and molecules in an electronic excited state, which are just one of the many transient intermediates that play an important role in photodynamic therapy for cancer treatment. They chose rose bengal, a halogenated xanthene dye (4,5,6,7-tetrachloro-20,40,50,70-tetra-iodofluorescein di-sodium salt), which has a strong absorption at 532 nm. This particular molecule has a 98% quantum yield of the intersystem crossing, meaning the excitons are almost entirely long-lived triplets. They observe an increased muon relaxation rate as a consequence of light irradiation. They conclude that muonium reactivity with solute molecules is modified when in their electronic excited states and that it would, in principle, be possible to study kinetic isotope effects as a function of

excitation energy. Finally, they note that future studies may employ a tuneable laser source to allow excitation into the electronic absorption bands of a variety of molecules.

3. The future

3.1. The HiFi upgrade

The new high-field muon instrument at ISIS, called HiFi, provides applied longitudinal fields of up to 5 T. The magnet is a 5 T superconducting split-pair, with high field homogeneity over the sample volume and actively compensated stray field. It has additional z-axis coils up to ± 400 G for small changes to the main field (e.g. for sweeping through ALC resonances) as well as 100 G x- and y-axis transverse coils for calibration measurements. The 5 T magnet can access a range of accessible fluctuations, correlations, diffusion and dynamics across a broad range of systems, it can give access to new regions of magnetic phase diagrams and allow state preparation in, for example, frustrated systems, it can open up the full range of nuclei for RF-decoupling techniques and it can give access to level crossing resonances for spectroscopy and molecular dynamics studies.

Currently, it is not possible to perform laser excited muon spectroscopy with HiFi. The only muon spectrometer used for materials research that is equipped with a laser is the Argus spectrometer, part of the RIKEN-RAL facility at ISIS. However, this has a maximum magnetic field of less than 0.5 T, which limits some of the science available. Specifically, to access the wealth of science about electron dynamics in soft-matter systems, one needs to tune to ALC resonances which typically occur at magnetic fields greater than 1 T. Adding a laser on HiFi will enable this unique and entirely unexplored area of science to be accessed.

The MuSES project (see http://muses.ph.qmul.ac.uk/), funded by the European Research Council, will upgrade the HiFI spectrometer with a laser and associated infrastructure to allow time-resolved photo-μSR experiments to take place. The laser will be manufactured by Litron Ltd and have a tuneable wavelength (200–2400 nm, with normal operational range of 350–1064 nm) provided by a high-power Nd–YAG backing an OPO. The Nd–YAG will operate at 25 Hz and have 2.5 J per $\sim$5 ns pulse at 1064 nm. Between about 10 mJ and several hundred mJ per pulse will be available from the OPO, depending on the wavelength (but very little power will be available close to the OPO duplication point). The sample illumination will be switchable between the fixed wavelength Nd–YAG harmonics (1064, 532, 355, 266 and 213 nm) for high-power illumination and the lower power continuously tuneable wavelengths of the OPO. The laser system will have automated push-button operation wherever possible, such that manual intervention will only be needed if a major change to the set-up is required (e.g. changing from deep-UV to visible). This dial-a-wavelength operation will enable users to concentrate on the science of their material, rather than tuning the optics.

The laser will be housed in a light-tight cabin close to the HiFi spectrometer, with a beam line routed mostly underneath the floor to the spectrometer. A light tight box housing an optical breadboard is attached on the spectrometer so that the laser light can be sent into it from the back or the side to allow a variety of experimental geometries. The box is large enough to house the laser diagnosis equipments (e.g. power sensor and beam profiler) and various optics such as a Pockel's cell and wave plates to control the light polarization. HiFi has an extensive range of sample environment equipment, such as a dilution fridge (30 mK–300 K), a ^{4}He cryostat (1.5–300 K), a flow cryostat (4–400 K), a closed cycle refrigerator (10–600 K) and a reflector furnace (300–1500 K). Currently, none of these have openings to allow light onto the sample. Initially, the closed cycle refrigerator will be modified to allow light onto the sample, and there are currently no detailed plans to make any changes to the other sample environments. Modifications will be made to the other equipment as the scientific need arises. It is anticipated that a majority of soft-matter experiments will make use of ALCs in liquids to maximize signal to noise and to take advantage of spatial resolution intrinsic to this technique (see below), although exploratory solid-state experiments are also planned.

In order to match the light absorption with the muon stopping profile, considerable thought has to be put into the liquid sample cell design. There are two designs that are possible—light and muons both in from the front, and muons in from the front with light in from the back. The former design requires a window that is both optically transparent and sufficiently thin to ensure that the muons do not stop in it. Rough calculations revealed that a fused silica window no thicker than 200 μm meet both of these requirements, but upon testing a cell with this window, we discovered that the window was too fragile to be reliable enough on a muon experiment.

We have therefore designed a new sample cell with the muons entering the sample through a thin Ti or Al window in the front and the light through a much thicker (at least 2 mm) fused silica window at the back. We performed some preliminary Monte Carlo simulations of this cell design for 6,13-bis(triisopropylsilylethynyl)-pentacene (TIPS-pentacene) dissolved in chloroform as the sample, for different concentrations of the solution. The Al muon window was 100 μm. We used the freely available GEANT4 simulation software, which has been extensively shown to give accurate predictions of muon spectrometer behaviour [27, 28]. The results of the simulations compared to the light penetration/absorption as a function of solution concentration for a wavelength corresponding to one of the absorption peaks of TIPS-pentacene, are shown in figure 4. The light penetration length which is optimum for our photo-μSR experiments can then be estimated by a normalized product of the number of photons absorbed and the number of muons stopping at a given position in the sample, which is shown in the inset of figure 4. The peak is relatively broad, centred on 65 μm penetration length, corresponding to about a 45 mM concentration. If another peak was chosen, for example the absorption peak at 650 nm, then a solution concentration of around 10 mM would be optimum. Muonium experiments are often carried out in solutions with a similar concentration (typically 5 mM), but it's also worth noting that concentrations as low as 1 mM may be feasible for photo-μSR experiments. This is because the peak in signal (inset to figure 4) is relatively broad and our

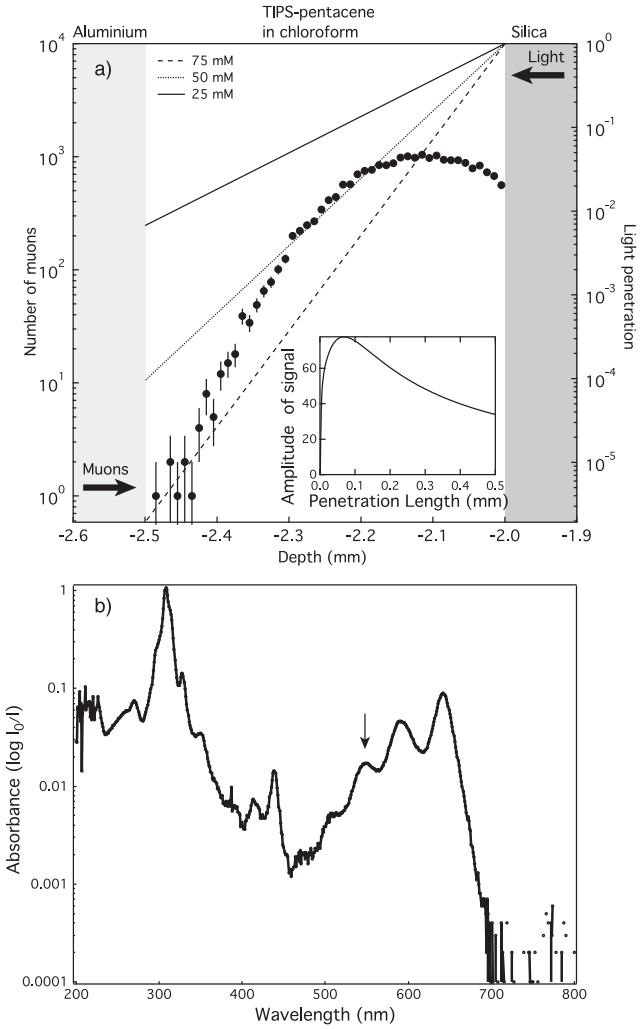

Figure 4. (a) Stopping profile of the muons (points; left axis) and the light penetration (lines; right axis) for different concentrations, plotted against distance for the new cell design. The inset shows a broad peak in light-induced signal strength at around 65 μm, which is easily calculated using the Monte Carlo simulations. (b) A typical UV–Vis absorption spectra for TIPS-pentacene in solution. The penetration of light (shown in a) was calculated for the wavelength at the absorption peak indicated by the arrow (approximately 550 nm).

calculations do not (yet) take into account the light scattering and reflecting from the muon window back into the sample cell. This would increase the signal amplitude at smaller light penetration lengths (i.e. lower concentrations). Clearly, these simulations are incomplete (e.g. we have not investigated how different thicknesses of Al window will modify results) and they have not been verified experimentally, but even at this early stage these simulations indicate the technique is feasible. This optimization will need to be carried out for every solute and/or solvent combination, prior to the muon experiments.

Finally, it is worth asking the question about whether we have enough photons for a sensible experiment. One might naively think that we would not be exciting enough molecules to have a measurable effect. Taking a laser power of 1 J per pulse at 532 nm (corresponding to the second harmonic of the Nd:YAG), we would have 2.7×10^{18} photons. With a sample volume of 0.5 c.c., a 10 mM solution would have 3.0×10^{18}, meaning we would be in the limit of enough photons for every molecule to be excited. With so many excited molecules, the sample degradation may be large for those materials where chemical reactions are photo-activated. Clearly, far from not having enough photons, we may actually have too many. This can be partially mitigated by a continuous flow of liquid through the cell, which is currently under construction. It will use a peristaltic pump to allow aggressive solvents to be used and the cell volume will be minimized to economize on the amount of sample needed. However, it is most likely we will also have to tune down the laser power to increase sample stability in those materials that are particularly prone to laser damage. We anticipate that not all materials will degrade during the week-long experiments, but also, that one must be particularly careful if UV light is used. Clearly, many of the details and questions about the experimental method will be clarified over the coming year, once the spectrometer is commissioned and the first experiments have been carried out.

3.2. Photo-excited μSR and ALC resonances

As described in the introduction, positively charged surface muons implanted into organic materials can either thermalize as bare muons with a positive charge, μ^+, or form a hydrogen-like species, known as muonium [1, 29–31], that can react with a molecule creating a radical state. Muonium can also sit in an unbound state in interstitial sites is known as vacuum muonium. Typically, in organic materials with unsaturated bonds, all three species are found, but it is the muoniated radical that is of most interest for photo-μSR experiments.

In a typical experiment to study muoniated radicals, a magnetic field is applied parallel to the muon's initial spin direction, and the energy levels of the singlet/triplet bound muonium states are tuned via the Zeeman interaction [1]. In high magnetic fields, where most experiments are carried out, the eigenstates of the spin systems are to a good approximation pure Zeeman product states. Muons injected with their spins parallel or anti-parallel to the field are thus in an eigenstate, and no time evolution of spin polarization is expected [32]. At a particular longitudinal field cross relaxation effects produce an ALC, at what would otherwise be energy level degeneracies, and eigenstates are mixtures between two Zeeman states. This leads to an oscillation between the levels. Whenever the two mixing levels belong to different muon magnetic quantum states, the time evolution causes a depolarization of the muon. The positions and linewidths of these ALC resonances are determined by the muon–electron isotropic and anisotropic HF coupling [1, 32]. The value of the isotropic muon–electron HF constant is determined by the overlap of the two wavefunctions, via the Fermi contact interaction. The muon's wavefunction is essentially a delta-function, whereas in muoniated radicals, the electron's wavefunction is spread over a large portion of the molecule. The degree of localization of the electron's wavefunction, where it is centred with respect to the muon and the electron's orbital angular momentum determines the value of the HF constant to the muon, and this varies considerably between different muon adduct sites, even ones that are next to each other on the same molecule. As a consequence, the magnetic field at the ALC strongly varies between sites, and

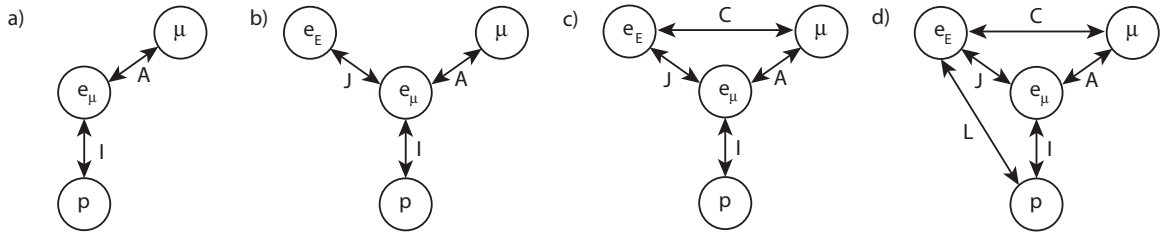

Figure 5. The various spin systems and coupling regimes of the photo-μSR experiments. (a) The ground state involving just three spins (proton, p; muonium electron, e_μ; muon, μ), which is the normal spin configuration in liquid experiments. HF coupling between the muon–electron is denoted A and coupling between the proton–electron is denoted I. Muon–proton coupling is normally neglected when modelling data. (b) The excited state, brought about via laser excitation, where second electron, e_E, is now coupled with the e_μ with a coupling denoted by J. The coupling of the excited electron to the muon and proton may be small. (c) It could be that the coupling between e_E to the μ cannot be neglected. This is denoted by C. (d) The worst case scenario, where the excited electron must also be coupled to the proton, denoted by L.

is readily calculable using, for example, density functional theory (DFT). Importantly, by tuning the magnetic field to a particular ALC resonance, one becomes extremely sensitive to the local spin environment surrounding the particular site that the muonium bonds to.

If the HF interaction is isotropic on the time scale of the experiment (e.g. the reorientation rate of the molecule is much larger than the dipolar part of the HF coupling, normally the case with a liquid), there are only muon–nuclear spin flip–flop transitions driving the ALC resonance [32], known as a Δ_0 transition. In solids, however, the dipolar part of the HF interaction drives two additional types of resonances, a single particle muon spin flip (Δ_1) and a muon–nuclear spin flip–flip transition (Δ_2). The latter is very weak, whereas the former is the most intense ALC in solid materials. The number, m, in Δ_m corresponds to the change of nuclear and muonic spin quantum numbers between the two degenerate states. The quantum mechanics of this three-spin system is none too trivial for the beginner [1, 32], but fortunately a robust, flexible and free software package called Quantum is available to perform calculations from the ISIS facility website [33] (see www.isis.stfc.ac.uk/groups/muons/).

In Δ_0 transitions, in addition to the muon–electron interaction, HF interactions of the electron with nearby hydrogens are also important in determining the positions of ALC resonances. When calculating ALC resonances, the multi-spin system of a typical molecule is usually simplified to a series of three-spin systems, each taking one of the protons or other nuclei and considering only the proton-electron and muon–electron coupling. This is depicted in figure 5(a), where the HF interaction constants are labelled A and I for muon–electron and proton–electron interactions, respectively. The direct HFC between the muon and proton is essentially zero since there is no wavelength overlap between the two localised particles, and the magnetic dipolar interaction is generally decoupled below a few mT, many orders of magnitude lower than the magnetic fields in a typical experiment. It is worth noting, that whilst the HF coupling between the proton and muon is small, the main interactions are mediated via the electron spin (therefore included) and dipolar coupling (averaged to zero in liquids; not needed for Δ_0 transitions).

The majority of the photo-μSR experiments on aromatic molecules or systems with double or triple bonds will be carried out in the liquid state (by making a solution of the

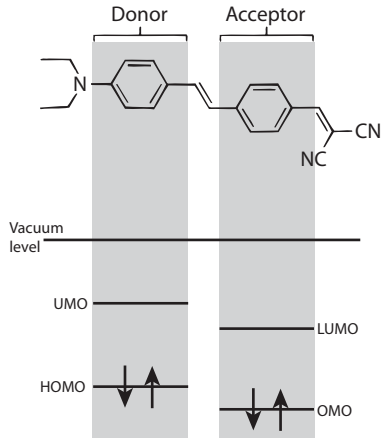

Figure 6. A stilbene derivative [34], explicitly showing the donor and acceptor parts of the molecule and a schematic energy level diagram that could describe this molecule. HOMO corresponds to highest occupied molecular orbital; OMO corresponds to occupied molecular orbital; LUMO corresponds to lowest unoccupied molecular orbital; UMO corresponds to unoccupied molecular orbital. The internal electric dipole moment results in the LUMO residing on the acceptor part of the molecule, whilst the HOMO resides on the donor part.

molecule), so will be mainly dealing with Δ_0 which are devoid of anisotropy in the muon–electron HF interaction. As discussed earlier, the reason for dissolving the molecule in a solvent is to ensure that the stopping distance of the muons (hundreds of μm) overlaps with the absorption of the light by the molecules (typically 10's nm in the solid state for many organic materials, although it will be clearly wavelength dependent). A careful choice of solvent is required to perform the experiments. Firstly, one must ensure that a good proportion of muonium is produced in the thermalization process. Secondly, the solvent itself must not form muoniated radicals; the muonium must thermalize as vacuum muonium. This means that if an organic solvent is used, it must be fully saturated. Thirdly, the solvent must be able to dissolve a suitable concentration of the molecule under investigation. Finally, the solvent must be optically transparent to the wavelengths used to excite the molecule under investigation. Examples of solvents that can be used are chloroform, dichloromethane, water, tetrahydrofuran, methanol and ethanol, although given the large number of organic solvents available, this is not an exclusive list.

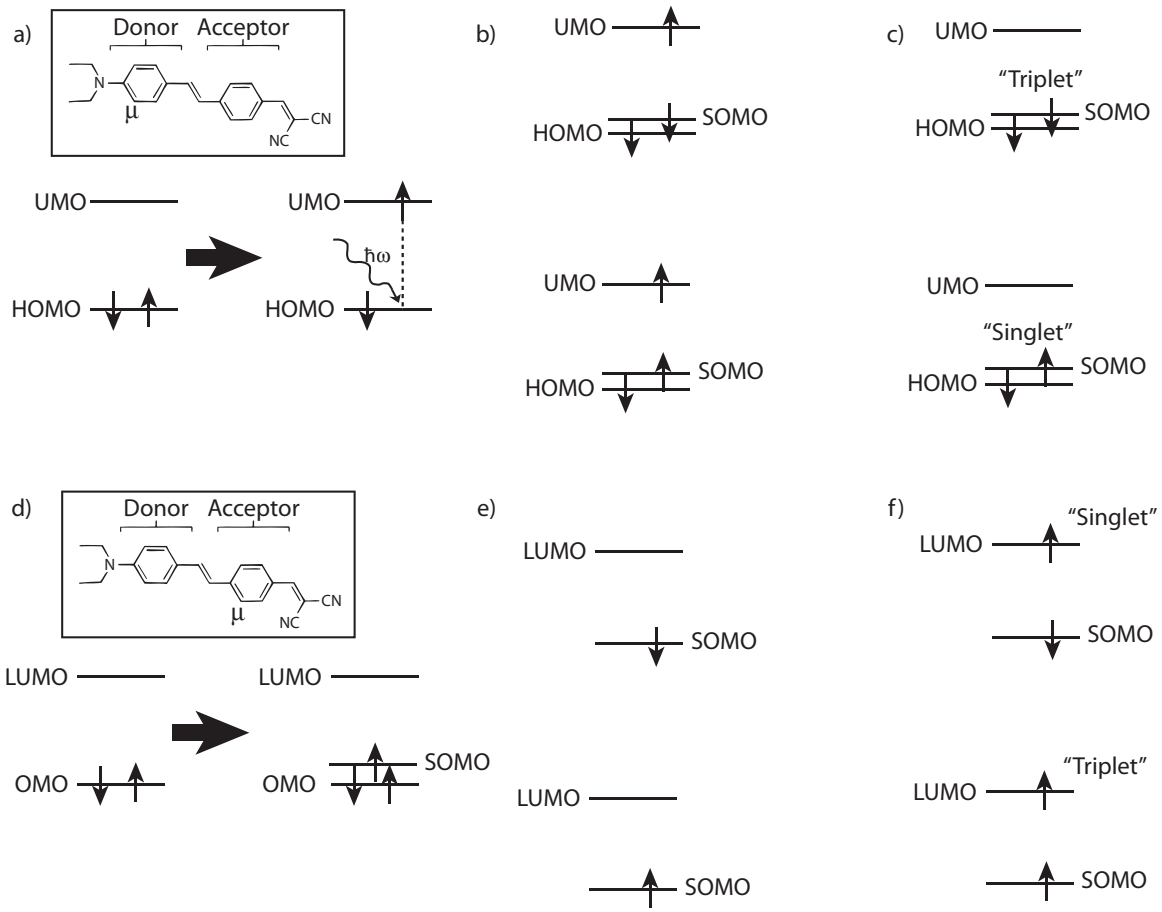

Figure 7. The measurement of the transient species, and the ultimate meta-stable state, are dependent on the position of the muon and the details of the timing of the pump–probe pulses. Proton and muon spins are omitted for clarity. (a) An electron is excited from the HOMO with a photon into an UMO on the donor side, then shortly after the muon bonds to somewhere on the donor side of the molecule. (b) If the excited electron is still present on the donor part of the molecule when the muon bonds, then the muon experiences a rather complex three-electron spin system. Two of the four possibilities are shown. (c) Once the electron has moved from the donor side, then the spin system will consist of two electrons. (d) This case is similar to the previous; the electron is excited from the HOMO to UMO (not shown), but the muon bonds to the acceptor part of the molecule before the electron has moved from the donor side. (e) As a consequence, the only electron that is coupled to the muon is the one in the SOMO. The HOMO has been omitted for clarity. (f) After some time, the excited electron moves from the donor to the acceptor part, and the muon is coupled to two electron spins.

In the photo-μSR experiments, it is anticipated that under standard operation, the laser light will arrive prior to the muons arriving. An electron is then excited in the molecule from the highest occupied molecular orbital (HOMO) to the lowest unoccupied molecular orbital (LUMO) when a photon is absorbed with an energy corresponding to the energy difference of the two. A muonium then bonds to the molecule once it is in this excited state, bringing in a secondary electron, which resides in a singularly occupied molecular orbital (SOMO) with an energy which is normally between the HOMO and LUMO but relatively close to the HOMO. Many molecules have an internal electric dipole moment, which can result in the LUMO and HOMO residing on a different part of the molecule. This donor–acceptor relationship is demonstrated in figure 6 for a stilbene derivative [34], the class of which is commonly used in dye-lasers due to their 'hyperpolarizability' resulting in nonlinear optical properties. Particularly in these systems where there is an internal electric dipole moment, the muonium adduct determines the nature of the spin system measured.

Shown in figure 7 are two possibilities of muonium addition to a simple molecule (the same molecule whose energy levels are sketched in figure 6). If the muonium adds to the donor part of the molecule (shown in the inset to figure 7(a)), then when an electron is photo-excited from the HOMO to an unoccupied molecular orbital (UMO) localized to the donor part, it is likely that this transient species (due to the electric dipole moment of the molecule) will transfer to the LUMO on the acceptor part. Since the electron's wave function is localized to the LUMO on the acceptor part of the molecule, the coupling constant between the muon and this unpaired electron is small. Then when the muonium binds to the molecule, the spin system is dominated by the electron brought by the muonium, residing in a SOMO, and the unpaired electron in the HOMO. If, on the other hand, the muonium is bound to the acceptor part (shown in the inset to figure 7(b)), then the spin system is dominated by the muonium electron in a SOMO and the unbound electron in the LUMO, which has been excited from the donor part and transfers to the acceptor part after some time. Similarly, the single electron in the HOMO on the donor part is only weakly coupled to the muon on the acceptor part, as its wave function is localized to a different part of the molecule. Clearly, both of these descriptions assume that the measurement takes place

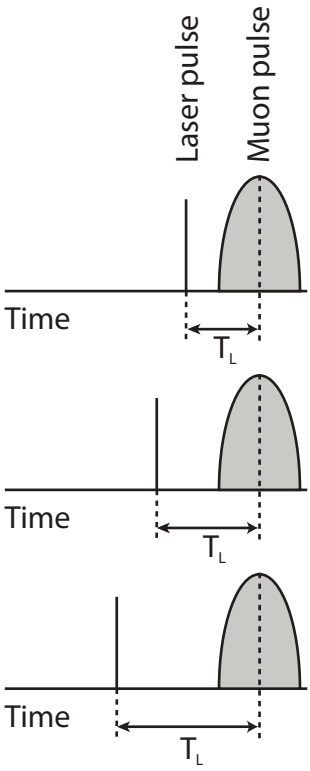

Figure 8. The pump–probe pulse structure. The pump (laser) timing can be changed relative to the probe (muons) to extract time dependence of the excitations.

at a time which is longer than the intrinsic timescale of the electron transfer (ET) from donor to acceptor. If it is not, it is likely that the spin system will be significantly more complex, although time-resolved studies will be quite interesting to carry out. Furthermore, it could be that when the molecule is in the excited state, the muon may not bind to the molecule in the same way as it would when it is in the ground state. A combination of quantum chemical calculations and experiments to probe this is dearly needed; once the spectrometer is built, investigating muonium physics in the presence of excited states will be top-priority.

In addition to this spatial resolution, photo-μSR is also able to measure the dynamical response of the excited electron. This can be achieved in two ways. The first is intrinsic to the muon spectroscopy technique; that is, observing how the muon's spin polarization evolves as a function of time from the laser pulse arriving. This would normally involve the laser pulse arriving just before the muon pulse, to ensure that the muon is not involved in any excitation, and would have a maximum time resolution set by the muon half life combined with counting statistics, with most experiments reaching the useable data limit by perhaps 20–30 μs. The second method, which would perhaps be easier to interpret, involves changing the pump–probe timing T_L, as depicted in figure 8. One would increase T_L with a delay-generator, and then simply plot the muon relaxation or asymmetry as a function of T_L to extract the intrinsic time response of the electronic excitation. In addition to increasing the maximum time from tens of microseconds to 20 ms (ISIS runs at 50 Hz), this method offers the advantage that one does not have to quantitatively interpret the muon's spin relaxation rate directly to extract excitation dynamics. Indeed, it may be the default mode of operation, even for excitation timescales of 100's ns.

It is therefore possible to gain spatial resolution by tuning the magnetic field to a particular resonance on one particular part of the molecule, and temporal resolution by changing T_L. One is able measure how an excited electron's wavefunction evolves with time on different parts of a molecule—in other words, tracking the movement of an electron within a molecule. This spatial and temporal resolution, on sub-molecular length-scales, is quite unique and could yield valuable information about many processes that are not fully understood. Some of the potential applications of photo-μSR are discussed in section 4.

3.3. Modelling ALC resonances in the presence of excitations

As noted above, the presence of an excited electron can essentially be thought of as two electrons that may couple to the muon, and this two-electron system could be in a 'singlet' or 'triplet' state, determined by their relative spin orientation. As the first approximation of this singlet/triplet electron system one might wish to perform standard liquid Δ_0 ALC simulation (depicted in figure 5(a)), but make the electrons' spin either one or zero, representing the triplet and singlet state respectively. It is only a valid approximation if the two electrons are in the same orbital; they must then by definition have the same interaction with the muon and other spins in the system, and it is legitimate to then modify the total spin rather than treat each electron individually. This is clearly impossible for the triplet case. For the case where the electrons have antiparallel spins and are in the same orbital, the two electrons would be in the singlet state, resulting in a diamagnetic molecule and no ALC resonance or low-longitudinal-field repolarization.

If the two electrons are in different orbitals, which must be the case if their spins are parallel (i.e. a triplet) and is likely even for a singlet, then they will have different couplings to the muon and other spins, as well as some coupling J between them. Given the Δ_0 transition in the liquid *must* involve a proton coupling to the muonium electron, one therefore must move from a three-spin system involving a muon, proton and electron that is somewhat trivial to calculate, to a rather more complex four spin system. Shown in figures 5(b)–(d) are three possibilities for the coupling mechanism in this four spin system. The first, in figure 5(b), involves just putting in an additional coupling J from the excited electron, e_E, to the muonium electron e_μ. The second, shown in figure 5(c), has an additional coupling C between e_E and the muon. The final one, shown in figure 5(d), has another coupling between e_E and the proton. Currently, it is not possible to calculate either of the two more complicated cases with Quantum (shown in figures 5(c) and (d)), although future developments of the Quantum software may make this possible.

To investigate the role of J, the coupling between the two electrons in the system, we have therefore chosen to use the case depicted in figure 5(b). This may be a reasonable approximation given J will be proportional to the product of the two magnetic moments of the species involved, although we expect that coupling between the second electron and

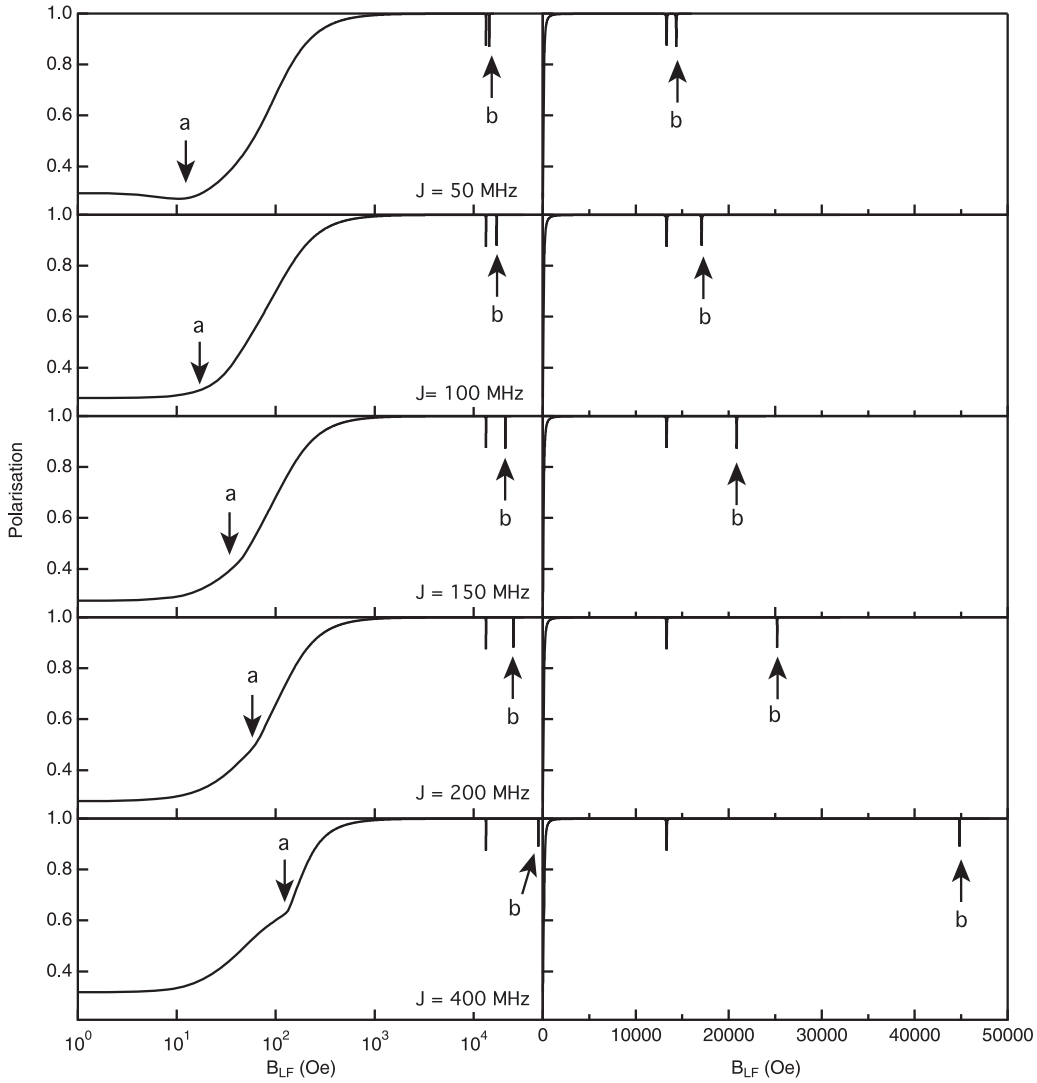

Figure 9. The evolution of the muon's polarization as a function of electron–electron coupling constant, J, plotted on a logarithmic and linear scale (left and right, respectively). J is shown in the label for each row, $I = 50$ MHz and $A = 300$ MHz. The higher J modelling can be found in figure 10.

muon will result in more complex signals. We have not explicitly forced either a spin-aligned or spin-anti-alligned state on the system, but assumed a statistical distribution of spin orientations. Shown in figure 9 is how the polarization of the muon changes with coupling constant J, in the low coupling limit, on both a logarithmic and linear scale. There are several features to note. Firstly, the normal Δ_0 resonance position at about 13 kOe, corresponding to the ground-state Δ_0 resonance, does not change position, amplitude or shape when J is modified. The most important feature shown in figure 9 is the evolution of *two* additional ALC resonances. One is at low magnetic field which is labelled as ALC_a, which slowly evolves to higher magnetic fields as the coupling constant is increased, and is best observed when the magnetic field is plotted on a logarithmic scale. At certain values of J, ALC_a is rather difficult to observe since it is at the same position as the knee in the repolarization curve. The other, labelled as ALC_b, splits from the original ground-state ALC and rapidly increases its position until it disappears off the scale, beyond the maximum field of the HiFi spectrometer.

Shown in figure 10 is how the polarization of the muon changes with coupling constant J in the intermediate coupling limit. It has been plotted with both a logarithmic and linear x-axis scale, to enable changes at both low and high magnetic fields to be observed. As can be readily observed in the figure, the resonance field of ALC_a slowly increases as the coupling constant J is increased. It eventually has a position that exceeds the maximum field of the HiFi spectrometer, at around 150 000 MHz for the values of A and I chosen to perform the calculation. The shape of the spectra does not change over the entire range of J chosen.

We would like to note that whilst a J of 150 000 MHz might appear to be rather large, it is still nonetheless in the intermediate coupling regime. Moreover, we expect to be in this intermediate coupling regime for the majority of the experiments. One can get an understanding on the order of magnitude of the electron–electron coupling constants in the high-coupling limit by using vacuum muonium as an example. Vacuum muonium has an isotropic HF coupling constant of 4463 MHz, significantly higher than the muoniated radical HF constants as the electron's wavefunction is not spread over a molecule. Given the coupling constant is proportional to the product of the two magnetic moments of the spins that are coupled, the high-coupling limit of J is therefore about

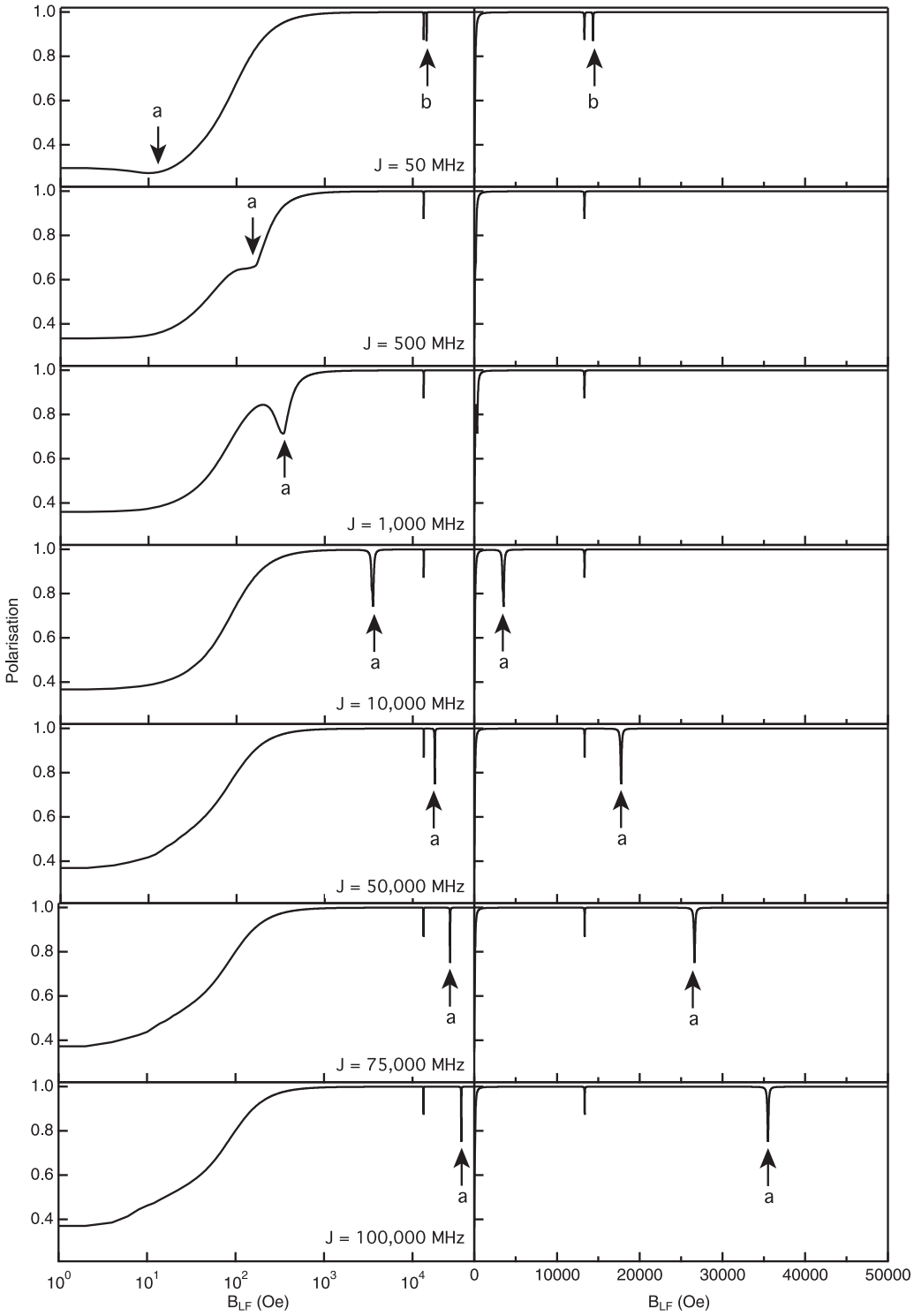

Figure 10. The evolution of the muon's polarization as a function of electron–electron coupling constant, J, plotted on a logarithmic and linear scale (left and right, respectively). J is shown in the label for each row. As a continuation of the modelling shown in figure 9, the nuclear and muon HF constants are the same as before: $I = 50$ and $A = 300$ MHz.

1 THz (about 200 times 4463 MHz). However, given that in most organic molecules, the electron's wavefunction is not a delta function but is spread over a portion of the molecule, we would expect to be in the intermediate coupling regime for many experiments. For example, for a standard muoniated radical state, the muon–electron HF constant is typically a few hundred MHz. Assuming a similar spatial extent to the second electron's wavefunction, we might expect J therefore to be no more than 10 000–100 000 MHz in most experiments. The low coupling limit, where J is in the tens to hundreds of MHz range, would be observed when the muon is located on a portion of the molecule where the electron's wavefunction does not strongly overlap with the muon's. This could be the case when the muon is located on the donor part of a molecule and the electron's wave function is localized to the acceptor part of the molecule, or vice versa.

Given the muon's polarization appears to be quite a complicated function of J and magnetic field, a useful

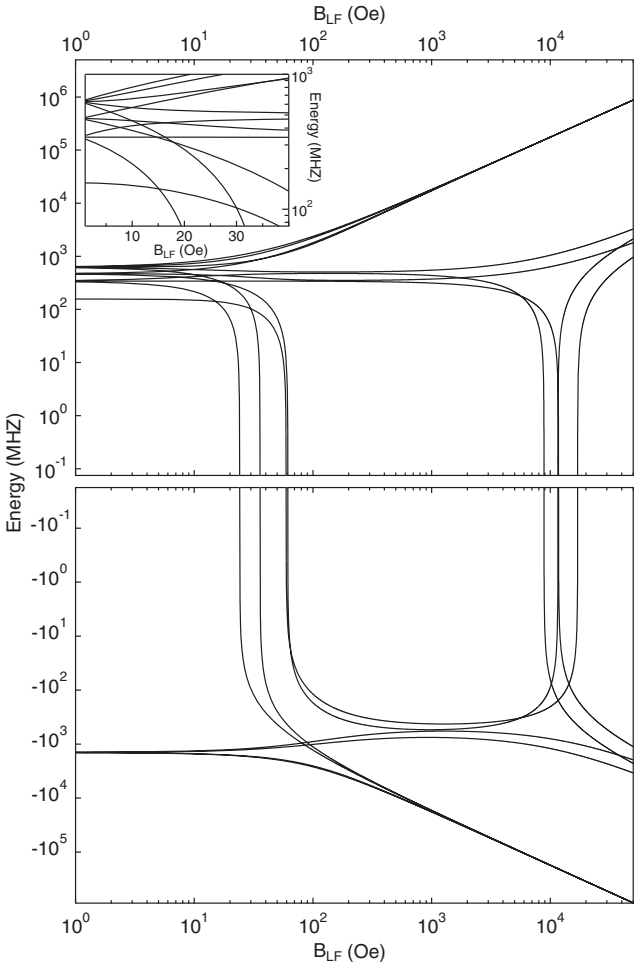

Figure 11. The Breit Rabi diagram for the same four spin system calculated in figures 9 and 10, with $A = 300$, $J = 50$ and $I = 50$ MHz. The top panel is a plot of the 'positive energies', the lower panel is a plot of the 'negative energies', achieved by reversing sign to enable plotting on a logarithmic scale. The crossing of the lines through zero is of no significance. The inset of the top panel is a plot of the low-field region, where it is clear that there are many level crossings, some avoided, others not.

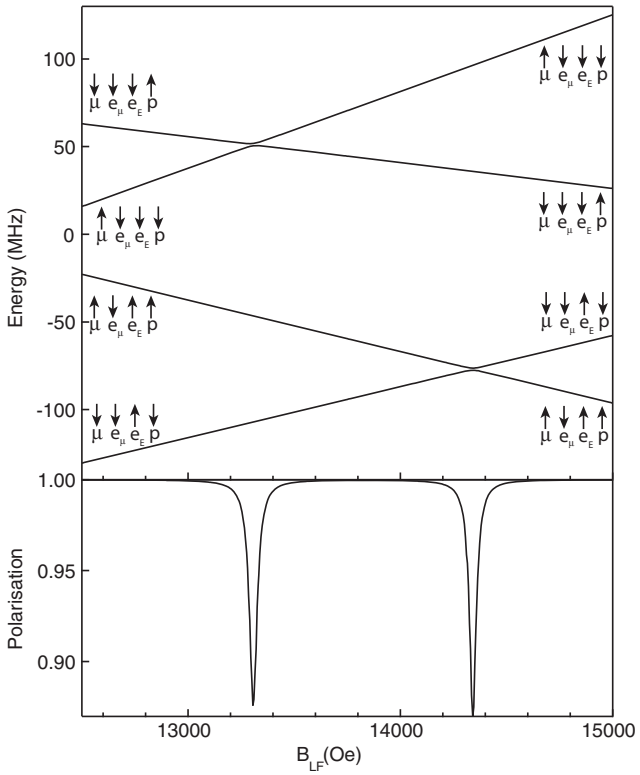

Figure 12. The two ALCs responsible for the loss of polarization of the muon, for $A = 300$, $I = 50$ and $J = 50$ MHz. The upper level crossing has had a linear background subtracted from it (with the gradient mainly determined by the electron gyromagnetic ratio) to enable it to be easily plotted. The spin polarization of the four spins in the system is schematically shown at low magnetic fields below the resonance field and at high magnetic fields above the resonance field.

exercise would be to identify what resonance corresponds to what combination of spins. Shown in figure 11 is the Breit-Rabi diagram for the four spin system with $J = 50$ MHz, and as expected, there are sixteen energy levels with *many* level crossings. Some of them are true crossings, i.e the levels do not interact at all. Others are avoided crossings, which either do not involve the muon's spin and so are invisible to the technique or do involve the muon's spin, which result in the loss of the muon's spin polarization (observed in e.g. figure 12). The number of level crossings, avoided or otherwise, is particularly clear in the inset to figure 11.

It is worth noting that these calculations were performed in the absence of anisotropy, as is expected for liquid state measurements, so it is likely the resonances observed (in figures 9 and 10) are due to transitions between spin states that have opposite muon and 'other' spins, mixed by the isotropic HF interaction (a muon-'other' spin flip–flop transition). We first investigate the ALC resonances in the low-coupling (small J) regime. The Δ_0 transitions are confirmed by consulting the polarization of the four individual spins in the system as a function of magnetic field through the resonances. As shown in figure 12, for both of the resonances, the two electron spins do not change; they both involve only the muon and proton. Since the Δ_0 transition at approximately 13 kOe is present in the ground state and it does not change with J, it must therefore be a muon–proton spin flip–flop transition. In this case, the two electrons have their spins aligned. ALC$_b$, on the other hand, is not present without the second electron and scales with the coupling constant J. It is also a muon–proton spin flip–flop transition, but with the electrons in a state with their spins anti-aligned. As expected, the ALC position shifts as I is changed, shown in figure 13.

ALC$_a$ is somewhat more complicated. Eight energy levels are plotted in figure 14, where it can be seen there are a variety of level crossings and ALCs, some of which involve the muon's spin and others do not. Of the eight lines plotted, there are six involved in four avoided crossings. Given the complexity of the Breit-Rabi diagram, it is rather complicated to represent the spins for the relevant avoided crossings on figure 14 itself. They are therefore shown in table 1.

There are two overlapping broad avoided crossings (lines 3–5 and 4–6) which correspond to a muon spin flip combined with an electron transition between aligned and anti-aligned spin states. These are similar to a traditional Δ_0, but involve electrons rather than protons and would be straight-crossings if it were not for the muon and proton. There is one line for each proton spin state. The line position, and possibly width,

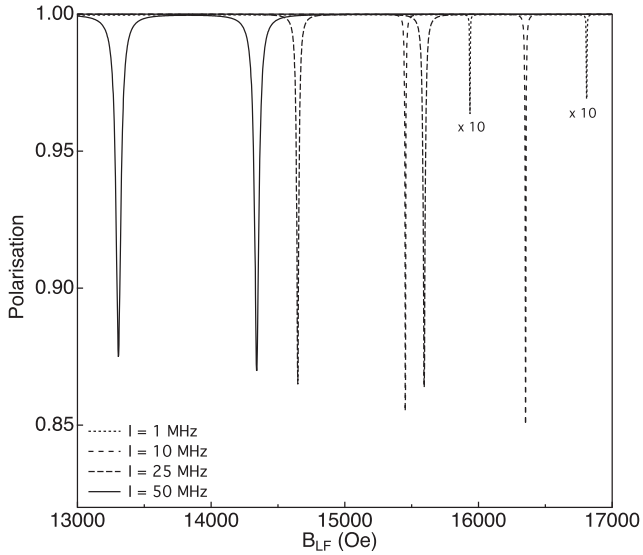

Figure 13. The evolution of the muon's polarization as a function of electron–proton coupling constant, I. The electron HF coupling constant was chosen to be a convenient value to investigate ALC_b and the muon HF constants are the same as before: $J = 50$ and $A = 300$ MHz.

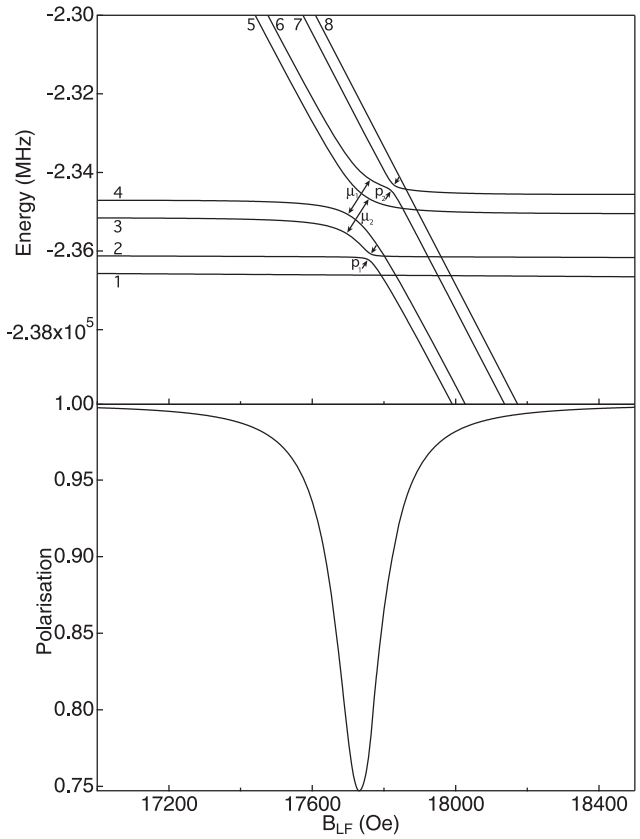

Figure 14. A number of level crossings and ALCs, for $A = 300$, $I = 50$ and $J = 50\,000$ MHz such that it is in the intermediate coupling regime. There are four ALCs present. There are two broad crossings involving a muon spin flip and the two electrons, labelled by μ_1 and μ_2, and two sharper avoided crossings involving a proton spin flip and the two electrons, labelled by p_1 and p_2. Table 1 shows the spins of the avoided crossings involving the muon.

strongly depends on J and may not be as easy to measure in practice if J is fluctuating due to molecular motion. This effective broadening will likely be more pronounced when J is large, as in this case, so in an experiment it may be easier to measure the low-coupling regime resonance.

Table 1. The spin configuration before and after the ALC resonance in figure 14. It should be noted that, due to the presence of the narrow avoided crossings p_1 and p_2 which have two lines in common with μ_1 and μ_2, the final state of the joint lines (3 and 6) is relatively difficult to extract from the calculations. The spin states for lines 3 and 6 were inferred by comparing the ALC, Breit-Rabi diagram and spin states of this four-spin system with a three spin system without the proton. The states reported in this table for lines 3 and 6 correspond to the states that would be the case if it were not for p_1 and p_2.

			Spin state before	Spin state after
Lines	Label	Line	$\mu e_\mu e_E p$	$\mu e_\mu e_E p$
3–5	μ_2	3	↑ 0 0 ↓	↓↑↑↓
		5	↓↑↑↓	↑ 0 0 ↓
4–6	μ_1	4	↑ 0 0 ↑	↓↑↑↑
		6	↓↑↑↑	↑ 0 0 ↑

There are also two narrow avoided crossings, involving lines 2–3 and 6–7, which are not visible in the muon polarization. They are also an electron aligned to anti-aligned spin transition but involve a proton spin flip (this is also similar to a Δ_0). Since they do not involve the muon's spin, they have not been presented in table 1.

Clearly, the exact details of the spins and ALC resonances will be dependent on the spin system that is calculated and present in the experiments. The modelling presented here may not be an accurate portrayal of a real experiment. It could be significantly more complicated than this when, for example, one turns on the interaction between the second electron e_E and muon. The presence of an excited electron could also result in an increase in the electron spin relaxation rate, which results in a dramatic increase in ALC amplitude [35–37]. Moreover, the muonium adduct will probably be altered by the presence of an excited electron, as well as the conformation of the molecule or bonding probability. Whilst some may consider this uncertainty to be a problem, it is in fact quite the contrary; *any* observable change in the ALCs or off-resonant repolarization curve, which can be tracked as a function of T_L, means the electronic dynamics of excited states of the material can be measured. If one is mainly interested in the material properties, then the exact nature of the muonium state is somewhat less important. Watching qualitative trends of the muon's spin can result in quantitative information about the sample, due to the ability to alter T_L. Indeed, this modelling clearly demonstrates that muons are extremely sensitive to the local environment in which they sit, which is exactly what we need to perform a successful experiment.

4. Potential applications

4.1. ET in amino acids and proteins

One particularly interesting area that photo-μSR can be used to probe is ET in proteins and peptides. Such charge transfer processes play a central role in many biological phenomena ranging from enzymes function to photosynthesis. They are fundamental for all living organisms, being key steps in the function of several natural enzymes including

cytochrome c, participating in ATP synthesis, DNA photolyase and ribonucleotide reductase, that contribute to DNA synthesis and repair, and photosystem II, the latter being the heart of natural photosynthesis [38–40]. Due to the complexity of a protein matrix, the study of an ET single event in the sequence of reactions occurring in these phenomena is a formidable task but fundamental for their understanding. Hence, the role of amino acid radicals as intermediates in ET is a topic of growing interest and research activity in fields as enzymology or energy studies, with the aim of clarifying the key steps in phenomena whose understanding could lead to revolutionary change in medicine or energy production.

In the first μSR experiments on proteins, off-resonance measurements were performed, using the Risch–Kehr formalism (a model originally developed for the polaron motion along polymer chains) [41] to extract the one-dimensional (1D) diffusion rates of electrons on the backbone of the protein. For example μSR measurements have been performed on cytochrome-c, a protein involved in the respiratory electron transport chain in mitochondria [42, 43, 45]. They observe two regions with different field dependencies of the RK relaxation parameter: a weak dependence at low field and the inverse dependence expected for 1D motion of the electrons at higher fields. They explain these results in terms of a 1D motion and attribute the cutoff, in analogy to previous observations in polymers, to an increase in the effective dimensionality of the motion at high temperatures due to an increased inter-chain diffusion rate [42, 43]. The same method has been applied to other proteins, such as ferritin and myoglobin, and similar results have been observed [42–44]. In these first studies of charge transfer in proteins using μSR, in analogy to that observed in polymers, the excitation is induced by the presence of the muonium itself. However, this kind of approach gives limited information about ET. There is no spatial resolution, despite the technique being an intrinsically localized molecular probe, as all of the work has been conducted in magnetic fields that are off-resonance and the signal measured is a superposition of all possible muonium sites in the system, which would be numerous in the molecules measured. One is not therefore able to identify, for example, the donor and acceptor sites, as well as any possible intermediate state. Moreover, little is known about the muonium states themselves that give rise to the excitation, as it is extremely challenging to access the detailed information required on the multiple muonium sites from the off-resonance longitudinal field repolarizations. Details such as the relative formation probability of the different muonium sites and their HF coupling constants are required as input parameters to the quantitative analysis, but these are rather difficult to extract from off-resonance studies. However, all of this information can be found by studying the ALC resonances, which are located at significantly higher magnetic fields than available on most spectrometers.

ET in proteins is usually studied by time resolved absorption techniques, with the main aim of characterizing the rate of the charge transport and its relation with the composition and length of the polypeptide chain. Laser flash photolysis induces the radical formation and a subsequent detection of the transient species having a well defined absorption band, whose lifetime is often in the ns to ms range. These studies have resulted in many insights into ET processes in proteins in the last few decades, but there are limitations, as the optical properties of the sample can be non-ideal (e.g. overlapping excitation energies of the ground state and absorption energies of the excited species) and like off-resonance μSR, only average information over the entire molecule can be obtained. This means no spatial information can be directly obtained from these techniques, although indirect means, such as chemical substitutions, are often employed. It is therefore rather difficult to track the electron's progress through the molecule, making it challenging to identify the exact nature of the transfer mechanism.

ET processes between electron donors and electron acceptors are usually described either by the superexchange theory (or electron tunnelling) or by the electron hopping model [46]. Electron tunnelling is a one step process which falls off strongly with distance. The hopping model provides an explanation for ETs across long distances, but it is dependent on the presence of suitable redox intermediates, which serve as stepping stones between electron donors and final electron acceptors [46].

Whilst an ET hopping pathway using aromatic amino acids as stepping stones has been proposed in some enzymes (such as ribonucleotide reductase or DNA photolyase [38, 47–49]), there is insufficient information about the specific role that the 21 individual natural amino acids have on ET. Clearly, the driving force behind ET is a reduction in free energy of the charge carrier involved, but the standard oxidation potentials of the donor, acceptor and any stepping stones are only rough estimates for the ET free energy. One role that amino acids can play is simply structural, where the specific combination of amino acids in the peptide chain adjusts distance between the sites undergoing ET. For example, the polyproline II helix has a transition between a single-step tunnelling and a stepwise hopping (multiple tunnelling events) when the number of the units between the electron donor and the electron acceptor is larger than four [50]. Measurements in synthetic donor–bridge–acceptor complexes have shown that electrons can be transferred across 15 Å in microseconds [51] via several units. A gradual decrease in rate with distance was observed and attributed to tunnelling via hole and electron states of the intervening bridges, significantly increasing the range of single-step super-exchange mediated ET. However, there are clearly fast ET processes in large-molecules, where distances are larger than 15 Å (e.g. ET in photosynthesis takes a little more than 100 ns). So the question that must be asked with regard to proteins is, how does the heterogeneous array of bonded and non-bonded contacts in a folded polypeptide mediate long-range electronic coupling? Perhaps this is as result of alignment due to the Coulomb interaction, where a segment of a chain (e.g. with positively charged amino acid) helps orient the molecule towards another segment of the molecule (e.g. with negatively charged amino acids).

The combination of μSR with laser excitation has several unique advantages over the traditional optical pump–probe techniques. Firstly, the probe (muon) is totally independent of the pump (laser); there are cases where the absorption band of the excited state overlaps with the excitation, making flash photolysis experiments challenging. Perhaps most

importantly however, is that if one tunes to an ALC resonance, then site specific information on electron dynamics can be gained. The position where the muonium binds to the molecule determines the magnetic field at which the ALC is present and is readily calculable using DFT. Using photo-excitation on the HiFi spectrometer, which can access the high magnetic fields needed to measure the individual ALC resonances associated with each muonium bonding site, it will be possible to track the time evolution of the excited electron over the molecule at different positions on the molecule. It will thus allow the time it takes the electron to hop between each individual stepping stone in the transport chain to be measured and allow any steps that are skipped to be identified (i.e. it can differentiate between the superexchange theory and the electron hopping model directly). It can also identify bottlenecks in the transport chain, brought about by specific combinations of amino acids, and the reason behind these bottlenecks.

4.2. Photochemistry

Photochemistry is the study of chemical reactions that are brought about by the absorption of light by atoms or molecules. In addition to bringing to the molecule the necessary activation energy, the absorption of a photon by a molecule may also permit a reaction to occur by changing the symmetry of the molecule's electronic configuration, enabling an otherwise inaccessible reaction path. The reactions are normally several orders of magnitude faster than thermal reactions, although often they are still within the time window of the photo-μSR technique.

Many important processes involve photochemistry. The obvious example is photosynthesis, in which solar energy converts carbon dioxide and water into glucose, disposing of oxygen as a side-product (as already noted, ET is vitally important too). Another example is vitamin D3 (cholecalciferol), which is produced photochemically from 7-dehydrocholesterol in the skin of most vertebrate animals, including humans. Photochemistry can also be highly destructive. For example, medicine bottles are often made with darkened glass to prevent drug photodegradation. The generation of singlet oxygen by photosensitized reactions of triplet oxygen is also important. The resulting singlet oxygen is an aggressive oxidant, capable of converting C–H bonds into C–OH groups. In particular, the photosensitized production of singlet oxygen has significance in a range of areas from photooxidation, DNA damage, photodynamic therapy of cancer and polymer science [52].

One particular class of materials of interest for the first generation of photo-μSR experiments are the carotenoids. This class of molecules have their biochemistry linked to the lipids and to the lipid/water interfaces, including membranes. The increasing interest in their chemistry is related to the many functions of these biomolecules as a direct result of their rich structural diversity [53–56]. Many of these functions are only poorly understood, although carotenoids seem to be an integral part of the inherent defence against oxidative stress in plants and animals, as quenchers of singlet oxygen and as radical scavengers [57, 58]. For example, epidemiological studies have suggested that dietary β-carotene and lycopene may inhibit certain types of cancer. The potential anti-oxidant properties of carotenoids may also help to inhibit the onset of other diseases that are believed to be initiated by free radicals, including atherosclerosis, cataracts and multiple sclerosis [59]. As for radical scavenging, it is worth noting that carotenoid backbones are almost exclusively all trans-conjugate polyenes and are linear molecules, and they may scavenge radicals and act as linear transmitters of radicals antioxidant protection of sensitive structures [60]. It has been demonstrated theoretically that some carotenoids, such as β-carotene, could be excellent electron donors, while others such as astaxanthin, good electron acceptors [61–66]. In these materials, redox reaction dynamics may involve ET.

But before we get to understanding the photochemistry of the carotenoids, we must first explore, and understand, the exciton physics of these molecules. In recent transient absorption experiments, β-carotene was illuminated by 355 nm and an absorption band is found at 516 nm which has been assigned to a triplet excited-state [60]. Kinetic analysis of the time evolution profile at 516 nm shows this triplet has a 1.5 μs rise time constant, which is comparable with the 5 μs slow formation known for the triplet excited state of zeaxanthin [67]. It is not obvious why such a clear and long-lived triplet exists in a molecule that should have a low intersystem crossing rate. It has been suggested that excited molecules may within their lifetimes interact with secondary photons [67], and this kind of multi-photon excitation may lead to a more efficient triplet formation. However, further investigations need to be performed to fully justify this conclusion, for example by measuring the laser power dependence to the triplet signal. Alternatively, a photo-excited muon spectroscopy study of β-carotene could offer important insight about the origin of this triplet signal. In particular, this could be achieved by tracking the temporal and spatial evolution of the transient species responsible for the peak in the absorption at 516 nm.

However, the dynamics of the excitons is only the beginning of the study of the rather complex photophysics and photochemistry of β-carotene. The following three reaction pathways for photo-excited β-carotene could be available for radical scavenging:

$$\begin{aligned}
&\text{HAT}: \beta\text{-Car} + {}^{\bullet}\text{OH} \rightarrow \beta\text{-Car(-H)}^{\bullet} + \text{H}_2\text{O},\\
&\text{ET}: \beta\text{-Car} + {}^{\bullet}\text{OH} \rightarrow \beta\text{-Car}^{\bullet+} + \text{OH}^{-},\\
&\text{RAF}: \beta\text{-Car} + {}^{\bullet}\text{OH} \rightarrow \beta\text{-Car-OH}^{\bullet},
\end{aligned}$$

where HAT corresponds to hydrogen atom transfer, ET to electron transfer and RAF to radical adduct formation. Spectral evidence has been presented for ET reactions leading to the carotenoid radical cation. For example, in the NIR region, a transient species with a lifetime of 2 μs and maximum absorption at 830 nm is observed, which has been assigned to a carotenoid/solvent complex [60]. It transforms into another species at 10 μs with a characteristic absorption maximum at longer wavelengths (> 900 nm). This transient has been assigned to the carotenoid radical cation and is a relatively stable intermediate oxidation product [60], and importantly, may be generated photochemically in electron-accepting solvents such as chloroform. It should be noted that chloroform is an ideal solvent for muon experiments, as it readily forms muonium which can then

react with the target molecules (in this case β-carotene) to form the muoniated radical needed to probe the molecule.

RAF with oxygen-centred radicals to a carotenoid adduct has also been demonstrated [68–70]. Recent time-resolved studies of the hydroxyl radical reaction with β-carotene shows a short-lived species (< 10 ns formation and 150 ns decay) support adduct formation upon reaction of β-carotene with phenoxyl radicals. Adduct formation is also suggested for reaction of β-carotene with peroxyl radicals of linoleic acid, as formed in lipid autoxidation [54].

However, HAT from carotenoids to oxidizing radicals to yield the neutral carotenoid radical has only been suggested, without spectral or any other direct evidence [70–73]. HAT is known to be involved in oxidation of unsaturated lipids [74] and a demonstration of hydrogen transfer from carotenoids to oxidizing radicals, perhaps with muons which are analogues of hydrogen, may contribute to a better understanding of carotenoids as antioxidants in membranes especially under extreme oxidative stress.

Importantly, the timescales of photo-excited reactions are compatible with the timescales of laser excited muon spectroscopy; for example, there is an unknown β-carotene transient species with a millisecond lifetime, the β-carotene radical adducts have a several microsecond lifetime, the β-carotene radical cation ion pair has a several hundred microsecond lifetime and the β-carotene radical anion has a few tens of microsecond lifetime [60]. This means the study, with spatial resolution, of redox reaction dynamics and pathways could be accessible in photo-μSR experiments, and given the similarities of muonium to a hydrogen atom, muons could be a route to demonstrating, and understanding, the HAT mechanism directly. Muons are particularly sensitive to the subtleties of chemical reactions, since the conformation and local spin species in its immediate surroundings have a huge effect on the muon–electron HF coupling constants, for example. And depending on the adduct site, different ALC resonances will be affected by these molecular changes in a different way, so by combining this positional sensitivity with the temporal sensitivity of the pump–probe technique, new insights could be gained from studying reaction dynamics with photo-μSR. However, it remains a challenge to calculate the effect that these photo-induced molecular changes have on the spin environment of each adduct site, and work on this challenge has only just begun.

4.3. Photo-induced magnetism

Photomagnetism is the change in magnetic state of a material by the application of light. This affect has been observed in a range of materials including molecular magnets, such as the CoFe Prussian blue analogue (PBA) [75, 76], cyano-bridged bimetal assemblies [77, 78], π-conjugated radicals [79] and biindenylidenediones [80]. For CoFe PBA and some cyano-bridged bimetal assemblies, which consist of two metallic centres joined via ligands, the change in magnetization occurs due to charge transfer between metallic centres via the ligands. For CoFe PBA, the charge transfer, or ET, band occurs between 400 and 600 nm, which is readily accessible by a number of commercially available laser systems.

There is now a wide range of molecular magnets that show photoinduced magnetism and most of them contain two metallic centres, the main elements pairs found are Cu–Mo, Co–Fe and Co–W [77]. For many of these cyano-bridged bimetal assemblies, the transition from diamagnet/paramagnet to ferromagnet/antiferromagnet occurs at low temperatures ($T < 50$ K). Photomagnets occur in many different topological patterns and structures, for example in just one review article on octacyanides, more than 50 different topologies are listed [81], belonging to zero-dimensional (single molecular magnet), one-, two- and three-dimensional structures.

One particularly interesting class of photomagnet is the octacyanometalate system [82], which is one of the more versatile building blocks, as the octacyanometalates can adopt different spatial configurations depending on their chemical environment and surrounding ligands [81]. This family of molecules can be synthesized into discrete magnetic molecules, or single molecular magnets, or onto extended three dimensional structures. Of particular interest to the photo-excited muon measurements are the copper octacynomolybdates. For example $Mo(CN)_6(CN\text{-}CuL_2)_2)$, where L = *N,N*-dimethyl ethylene diamine, is seen as a prototype for a broader range of octacynomolybdates compounds [83]. In this system, after photoexcitation with 406 nm light, the magnetic susceptibility of the $MoCu_2$ unit increases [84]. A number of mechanisms explaining the photomagnetic transition in the octacynomolybdates have been proposed. One particularly popular mechanism for the transition is suggested to be similar to the one in PBAs [85–87] and involves charge transfer from Mo to Cu: $Mo(4d^2)$–$Cu(3d^9)$ $\rightarrow$ $Mo(4d^1)$–$Cu(3d^{10})$ [77, 82, 88]. An alternative explanation has been proposed involving a local low–high spin transition on the Mo ion [84, 89], which has recently been supported by DFT calculations [83]. There is a shortage of experimental data on the electronic nature of this class of materials, and in some cases, the information that is available is contradictory [90]. X-ray absorption spectroscopy experiments on the $[Mo(CN)_2$ (CN Cu(Tren))$_6]^{8+}$ complex, where Tren = tris(2-aminoethyl)amine, are consistent with the charge transfer mechanism [91]. The photoinduced magnetic behaviour in this molecule is thermally reversible, implying that the system has to overcome an energetic barrier to recover its initial structure, which is also consistent with the charge transfer mechanism [92]. However, the electron spin resonance spectrum of a polymer with similar units shows a decrease of the Cu^{II} signal, but no signal of Mo^{V} ions is detected [93]. Alternatively, recent x-ray magnetic circular dichroism (XMCD) experiments on $[Mo(CN)_6$ $(CNCu(Meen)_2)_2]$ (Meen = *N*, *N*-dimethylethylenediamine) show evidence of the appearance of a high spin Mo^{IV} ion ($S = 1$) and the authors propose a new mechanism involving the generation of such $S = 1$ species and disregard the charge transfer mechanism in this case [84].

Very little work has been done on photo magnets with muon spin spectroscopy. Recently, a photo-active CoFe PBA was studied primarily in the non-illuminated state [94]. Illumination measurements were attempted at 5 K with LEDs, but there was no change in the spectra. This was put down

to the mis-match of the muons position, which is hundreds of μm below the surface of the material, and the absorbed light (and photo-induced molecules), which is likely much smaller. Possibly an increased light intensity would help, but this material would be rather challenging to study on the HiFi spectrometer, as the magnetic moment of Fe and Co would result in precession, or relaxation, outside the time window of ISIS.

What makes the copper octacynomolybdate system particularly interesting for a photo-μSR experiment at ISIS is the fact that it is Mo and Cu that are responsible for the magnetism. These are both low moment atoms, and recent XMCD measurements on a octacynomolybdate single molecule show that the Mo in the high-spin state has a magnetic field dependent magnetic moment, which rises to just over 1 Bohr magneton in a 5 T magnetic field [84]. XMCD measurements on a octacynomolybdate cyno-bridged network show a magnetic moment on the Mo atom of just 0.4 Bohr magnetons in a 5 T magnetic field [89]. These are within the time resolution of ISIS, which is not the case for many other photo-excitable molecular magnets, such as the PBAs.

Secondly, some of these molecules are cluster-based or are single molecular magnets, so they may be soluble. These systems will almost certainly form muoniated radicals, which means that when dissolved in the correct solvent, relatively low concentrations of solute results in a relatively high signal to noise (orders of magnitude greater than one would expect from estimations just involving the concentration). This is due to the high muonium scavenging efficiency, as is observed in measurements performed on organic semiconductor molecules in solution. One could therefore vary the concentration, and to a lesser degree the muon momentum (by degrading the beam with a suitable material), so that the light absorption can be tuned to overlap with the muon stopping distribution. Importantly, as well as studying the local magnetism of these systems below the photomagnetic transition temperature, photo-μSR has the unique advantage of being able to perform time-resolved measurements. Various experimental scenarios could thus be envisaged to investigate the spin dynamics at elevated temperatures, perhaps offering vital clues as to the underlying mechanisms behind these fascinating compounds.

5. Conclusions

The combination of μSR with laser excitation has several unique advantages over the traditional optical pump–probe techniques. Key to its applicability to will be the possibility to track the time evolution of the electron at different positions on the molecule, as a direct result of the positional sensitivity obtained by tuning to different ALC resonances with the magnetic field. This spatial and temporal resolution, to the best of our knowledge, is unrivalled.

Example of photo-μSR's applicability are many, and this paper can only discuss a few pertinent examples. In ET systems that are biologically relevant, such as peptides, it will be able to measure the time it takes the electron to hop between each individual amino acid stepping stone in the transport chain and allow any steps that are skipped to be identified. Initial measurements on polypeptides suggest that the muonium readily binds to the carbonyl bonds, which are very common in amino acids, and that each adduct site has different muon–electron HF coupling constant. The technique can therefore differentiate between superexchange theory and the electron hopping model directly. Moreover, if targeted amino acid substitutions are performed then the role of the different amino acids on ET can be assessed directly. This is a particularly exciting avenue to explore, as the role of specific combinations of amino acids and their order within a peptide chain can be investigated.

As already noted in the in-depth discussion of β-carotene, peptides are not the only biologically active molecule that can be investigated by photo-μSR. Radical reactions are responsible for a huge array of biological processes, and their chemical reaction dynamics can be investigated via photo-excitation. Indeed, photochemistry is a mature research field, as radical reactions (which can be brought about by photo-excitation and therefore studied) are thought to be related to, and possible triggers of, serious diseases such as cancer, atherosclerosis, cataracts and multiple sclerosis. Moreover, photochemistry is also a direct tool for fighting some of the very same diseases, for example via photodynamic therapy of cancer. Radical scavengers—antioxidants such as β-carotene—are also thought to help prevent these diseases, once again returning to cancer as a particularly important example. And although we have mostly limited ourselves in this manuscript to a discussion of the complexities of β-carotene, the photo-μSR technique is not limited to investigating just this molecule; it just happens to be a good starting point. For example, there are more than 700 naturally occurring carotenoids identified so far, and other biologically relevant molecules that may be of interest are the quinones, phycobilins and flavines. Indeed, there are an almost unlimited number of transient species, of biological relevance, that are still to be fully understood. Moreover, in addition to the actual reaction dynamics that can be measured with muons, one must also consider that often the physics of these transient radical species also involves ET from a donor to acceptor part of the molecule; photosynthesis here being the classic example. Given the available time on the muon spectrometer, it seems very clear that one must be careful about what problems should be tackled.

When considering the total time available on the spectrometer, perhaps photomagnets present less of a problem (unless it is competing with biology, of course). There are fewer photomagnets than biologically active molecules and biological systems are significantly more complex. Moreover, at least initially, there are some limitations on what systems can be investigated with photo-μSR using HiFi. For example, the relatively broad muon pulse places an upper limit on the precession frequencies that can be measured at ISIS, so only low magnetic-moment systems can be currently investigated. Perhaps in the future, packet-slicing (combined with an increased muon flux) will improve the frequency response of HiFi. Another limiting factor is the need to match the light stopping profile with the muon stopping profile, which implies the experiments are easiest in solution. This therefore limits the experiments to soluble single molecular magnets, so the investigation of materials that require long-range crystallographic order will not be

easy. These include metal–organic frameworks and crystalline metal–organic systems. The molecules must also react with muonium and create radicals, which limits materials to those with double and triple bonds, or aromatic rings. However, the obvious importance of performing photo-μSR measurements on molecular magnets is that time dependence is intrinsic to the technique, whereas many of the measurements previously reported have relied on quasi-static measurements, such as magnetization. Importantly, one would be able to go to well-above the transition temperature of the photomagnet and measure the relaxation dynamics, on a ns to ms timescale. These are quite unique measurements and have significant potential to improve our understanding of these materials.

Clearly, there are many opportunities for solving topical and important questions with photo-μSR, some of which are discussed in this paper. However, prior to many of the somewhat challenging experiments and systems explored here, a careful set of *simple* experiments on *very simple* molecules is needed. When backed up with extensive modelling, which would likely be much more detailed than the first attempt presented here, one should be able to understand the underlying muonium physics of excited states. Appropriate systems to explore could be relatively small, yet readily soluble organic semiconductors, where exciton physics is already well explored. Probably, these molecules should have a high intersystem crossing rate, either intrinsic or sensitized by the correct choice of solvent. However, in all likelihood, the temptation will simply be too great to start the more complex ones before finishing the simple experiments; the pioneering and unique nature of some of the possible experiments, particularly those involving the biology of life, means one simply cannot resist. Indeed, some of the ideas presented here, and others, are already in the planning stage.

Acknowledgments

The authors thank Dr F L Pratt for discussions about the modelling in this paper. AJD acknowledges the support of the European Research Council (ERC) for funding the project 'Muon Spectroscopy of Excited States (MuSES)', project number 307593.

References

[1] Patterson B D 1988 *Rev. Mod. Phys.* **60** 69
[2] Blundell S J 1999 *Contemp. Phys.* **40** 175
[3] Nagamine K 2007 *Introductory Muon Science* (Cambridge: Cambridge University Press)
[4] Schenck A 1985 *Muon Spin Rotation Spectroscopy: Principles and Applications in Solid State Physics* (Bristol: Adam Hilger)
[5] Yaouanc A and Dalmes de Reotier P 2011 *Muon Spin Rotation, Relaxation and Resonance* (Oxford: Oxford Science Publications)
[6] Blundell S J 2004 *Chem. Rev.* **104** 5717
[7] Lee S L, Kilcoyne S H and Cywinski R 1999 *Muon Science Scottish Universities Summer School in Physics* (Bristol: IOPP)
[8] Nuccio L, Schulz L and Drew A J 2013 *J. Phys. D: Appl. Phys.* submitted
[9] Koechner W 2006 *Solid-State Laser Engineering* 6th edn (Berlin: Springer)
[10] Kadono R *et al* 1994 *Phys. Rev. Lett.* **73** 2724
[11] Jayasooriya U A *et al* 2004 *ChemPhysChem* **5** 257
[12] Shimomura K *et al* 1999 *Hyperfine Interact.* **120** 595
[13] Torikai E *et al* 2000 *Physica* B **289** 558
[14] Bakule P *et al* 2012 *J. Phys. Chem. Lett.* **3** 2755
[15] Zutec I, Fabian J and Sarma S D 2004 *Rev. Mod. Phys.* **76** 323
[16] Yokoyama K *et al* 2009 *Physica* B **404** 856
[17] Knotz H *et al* 2006 *Appl. Phys. Lett.* **88** 241918
[18] Pankove J I 1965 *Phys. Rev.* **140** 2059
[19] Romero D *et al* 1990 *Phys. Rev.* B **42** 3179
[20] Kadono R *et al* 1994 *Phys. Rev.* B **50** 1999
[21] Yokoyama K 2009 *PhD Thesis* University of California at Riverside
[22] Yokoyama K *et al* 2012 *Phys. Procedia* **30** 231
[23] Lichti R L *et al* 2007 *Phys. Rev.* B **76** 045221
[24] Shimomura K *et al* 2012 *Phys. Procedia* **30** 224
[25] Chow K H *et al* 1995 *Phys. Rev.* B **51** 14762
[26] Ghandi K *et al* 2007 *Phys. Chem. Chem. Phys.* **9** 353
[27] Lancaster T *et al* 2007 *Nucl. Instrum. Methods Phys. Res.* A **580** 1578
[28] Sedlak K *et al* 2009 *Physica* B **404** 970
[29] Roduner E 1988 *The Positive Muon as a Probe in Free Radical Chemistry* (*Lecture Notes in Chemistry* vol 49) ed F Berthier, M J S Dewar, H Fischer, K Fukui, G G Hall and J Hinze (Berlin: Springer)
[30] Pratt F L 2004 *J. Phys.: Condens. Matter* **16** S4779
[31] Drew A J *et al* 2008 *Phys. Rev. Lett.* **100** 116601
[32] Keitzman S R *et al* 1995 *Chem. Phys.* **192** 189
[33] Lord J S 2006 *Physica* B **374–375** 472
[34] Breitung E M *et al* 2000 *J. Am. Chem. Soc.* **122** 1154
[35] Schulz L *et al* 2011 *Phys. Rev.* B **84** 085209
[36] Nuccio L *et al* 2011 *J. Phys.: Conf. Ser.* **292** 012004
[37] Nuccio L *et al* 2013 *Phys. Rev. Lett.* **110** 216602
[38] Aubert C *et al* 2000 *Nature* **405** 586
[39] Wittekindt C 2009 *J. Am. Chem. Soc.* **131** 8134
[40] Nugent J H A 1996 *Eur. J. Biochem.* **237** 519
[41] Risch R and Kehr K W 1992 *Phys. Rev.* B **46** 5246
[42] Nagamine K *et al* 2000 *Physica* B **289** 631
[43] Nagamine K 2002 *Eur. Phys. J.* A **13** 189
[44] Telling M T F and Kilcoyne S H 2012 *Phys. Procedia* **30** 86
[45] Scheicher R H *et al* 2003 *Physica* B **326** 30
[46] Cordes M *et al* 2009 *Chem. Soc. Rev.* **38** 892
[47] Ekberg M *et al* 1998 *Biol. Chem.* **273** 21003
[48] Rova U *et al* 1999 *J. Biol. Chem.* **274** 23746
[49] Li Y F *et al* 1991 *Biochemistry* **30** 6322
[50] Malak R A 2004 *J. Am. Chem. Soc.* **126** 13888
[51] Warman J M 1999 *Advances in Chemical Physics Part 1 Electron Transfer–from Isolated Molecules to Biomolecules* vol 106 p 571
[52] DeRosa M C and Crutchley R 2002 *Coord. Chem. Rev.* **233** 351
[53] Kispert L D *et al* 2001 *Chem. Lett.* **39** 148
[54] Guo J J, Hsieh H Y and Hu C H 2009 *J. Phys. Chem.* B **113** 15699
[55] Boon C S *et al* 2010 *Crit. Rev. Food Sci. Nutr.* **50** 515
[56] Suganuma K *et al* 2010 *J. Dermatol. Sci.* **58** 136
[57] Burton G W *et al* 1984 *Science* **224** 569
[58] Mortensen A *et al* 2001 *Arch. Biochem. Biophys.* **385** 13
[59] Edge R *et al* 1997 *J. Photochem. Photobiol.* B **41** 189
[60] Chen C H *et al* 2011 *J. Phys. Chem.* B **115** 2082
[61] Galano A 2007 *J. Phys. Chem.* B **111** 12898
[62] Galano A *et al* 2009 *J. Phys. Chem.* B **113** 11338
[63] Martinez A *et al* 2009 *J. Phys. Chem.* B **112** 16945
[64] Martinez A 2009 *J. Phys. Chem.* B **113** 4915
[65] Martinez A *et al* 2008 *J. Phys. Chem.* A **112** 9037
[66] Opstad C L *et al* 2010 *Eur. J. Org. Chem.* **2010** 4637
[67] Billsten H H *et al* 2005 *J. Phys. Chem.* A **109** 6852
[68] Mortensen A and Skibsted L H 1997 *J. Agric. Food. Chem.* **45** 2970
[69] El-Agamey A and McGarvey D J 2005 *Org. Lett.* **7** 3957
[70] El-Agamey A and McGarvey D J 2003 *J. Am. Chem. Soc.* **125** 3330
[71] Mortensen A 2002 *Free. Radic. Res.* **36** 211

[72] Liebler D C and McClure T D 1996 *Chem. Res. Toxicol.* **9** 8
[73] Woodall A A *et al* 1997 *Biochem. Biophys. Acta* **1336** 33
[74] Huvaere J *et al* 2010 *J. Phys. Chem.* B **114** 5583
[75] Sato O *et al* 1996 *Science* **272** 704
[76] Sato O 2012 *Proc. Japan. Acad.* B **88** 213
[77] Bleuzen A *et al* 2009 *Inorg. Chem.* **48** 3453
[78] Ohkoshi S I and Tokoro H 2012 *Acc. Chem. Res.* **45** 1749
[79] Matsumoto I *et al* 2009 *Chem. Eur. J.* **15** 11210
[80] Han J and Meng J B 2009 *J. Photochem. Photobiol. C: Photochem. Rev.* **10** 141
[81] Sieklucka B *et al* 2011 *Eur. J. Inorg. Chem.* **2011** 305
[82] Herrara J M *et al* 2004 *Angew. Chem.* **116** 5584
[83] Bunau O *et al* 2012 *J. Phys. Chem.* A **116** 8678
[84] Arrio M A *et al* 2010 *J. Phys. Chem.* C **114** 593
[85] Sato O 2012 *J. Photochem. Photobiol. C: Photochem. Rev.* **5** 203
[86] Bleuzen A *et al* 2000 *J. Am. Chem. Soc.* **122** 6648
[87] Moulin C D *et al* 2000 *J. Am. Chem. Soc.* **122** 6653
[88] Ma X D *et al* 2005 *Phys. Rev.* B **72** 094107
[89] Brossard S *et al* 2012 *J. Am. Chem. Soc.* **134** 222
[90] Carvajal M *et al* 2011 *Dalt. Trans.* **40** 7295
[91] Herrera J M *et al* 2008 *Phil. Trans. R. Soc.* A **366** 127
[92] Herrera J M *et al* 2004 *Angew. Chem. Int. Edn Engl.* **43** 5468
[93] Zhang W, Sun H L and Sato O 2010 *Cryst. Eng. Commun.* **12** 4045
[94] Salman Z *et al* 2006 *Phys. Rev.* B **73** 174427